The Adiabatic-Molecular Dynamics|generalized Vertical Hessian approach: a mixed quantum classical method to compute electronic spectra of flexible molecules in condensed phase

Javier Cerezo,[*,†,‡] Daniel Aranda,[¶,§] Francisco José Avila Ferrer,[§] Giacomo Prampolini,[*,¶] and Fabrizio Santoro[*,¶]

†*Departamento de Química, Universidad Autónoma de Madrid, 28049 Madrid, Spain*

‡*Institute for Advanced Research in Chemical Sciences (IAdChem), Universidad Autónoma de Madrid, 28049 Madrid, Spain*

¶*CNR–Consiglio Nazionale delle Ricerche, Istituto di Chimica dei Composti Organo Metallici (ICCOM-CNR), SS di Pisa, Area della Ricerca, via G. Moruzzi 1, I-56124 Pisa, Italy*

§*Universidad de Málaga, Andalucía Tech, Facultad de Ciencias, Departamento de Química Física, E-29071-Málaga, Spain*

E-mail: javier.cerezo@uam.es; giacomo.prampolini@pi.iccom.cnr.it; fabrizio.santoro@pi.iccom.cnr.it

Abstract

We present a general mixed quantum classical method that couples classical Molecular Dynamics (MD) and vibronic models to compute the shape of electronic spectra of flexible molecules in condensed phase without, in principle, any phenomenological broadening. It is based on a partition of the nuclear motions of the solute+solvent system in "soft" and "stiff" vibrational modes, and an adiabatic hypothesis that assumes that stiff modes are much faster than soft ones. In this framework the spectrum is rigorously expressed as a conformational integral of quantum vibronic spectra along the stiff coordinates only. Soft modes enter at classical level through the conformational distribution that is sampled with classical MD runs. At each configuration, reduced-dimensionality quadratic Hamiltonians are built in the space of the stiff coordinates only, thanks to a generalization of the Vertical Hessian harmonic model and an iterative application of projectors in internal coordinates to remove soft modes. Quantum vibronic spectra, specific for each sampled configuration of the soft coordinates, are then computed at the desired temperature with efficient time-dependent techniques, and the global spectrum simply arises from their average. For consistency of the whole procedure, classical MD runs are performed with quantum-mechanically derived force fields, parameterized at the same level of theory selected for generating the quadratic Hamiltonians along the stiff coordinates. Application to N-methyl-6-oxyquinolinium betaine in water, dithiophene in ethanol, and a flexible cyanidine in water are presented to show the performance of the method.

1 Introduction

Electronic spectroscopy is a ubiquitous tool in modern chemical research. Theoretical models and computational methods can greatly help to unveil all the information carried by the spectroscopic signal, allowing to establish a direct connection with the microscopic properties of the system under investigation.[1–3]

The quantum nature of molecular vibrations has a remarkable impact on the shape of electronic spectra. Although the most spectacular feature is the appearance of vibronic bands, an analysis in terms of moments[4] reveals that nuclear quantum effects (NQEs) are also important for structureless bands, modifying *e.g* their centre of gravity,[5] width[4,6,7] and asymmetry.[4] While for small systems in gas phase full anharmonic and nonadiabatic approaches are conceivable (see *e.g.* ref. 8), the treatment of large systems, including dozens or hundreds of vibrations, requires approximations. In the following we generically indicate as "stiff" systems, those for which quadratic expansions provide a reasonable description of the Potential Energy Surfaces (PESs) of the initial and final electronic states of the transition of interest. For harmonic PESs, and if couplings among the electronic states are negligible, the calculation of vibronic spectra is nowadays standard thanks to recent progresses in time-independent (TI)[9–13] and time-dependent (TD) approaches.[14–17] Both TI[12] and TD[12,18–23] schemes have been extended to account for intensity borrowing Herzberg-Teller (HT) mechanisms. These methods are efficient enough to be applicable to systems with dozens or hundreds of normal modes, as revealed in combination with cost-effective electronic methods like Density Functional Theory (DFT), and its TD extension (TD-DFT) for excited states.[24] Linear (LVC) and Quadratic vibronic Hamiltonians (QVC),[25] including quadratic diagonal potentials plus linear and quadratic off-diagonal couplings, provide a natural extension of the above models when interstate electronic couplings are important. With LVC and

QVC models, the vibronic spectra can be efficiently computed even for systems with dozens of normal modes,[26,27] by numerically propagating nuclear wavepackets on the coupled surfaces with powerful methods like MCTDH[28] and its multilayer extension (ML-MCTDH).[29,30] Anharmonic corrections[31,32] can be included in the vibrational frequencies, adopting second-order vibrational perturbation theory,[33,34] and taking benefit, for example, from the availability of analytic Hessians within DFT and TD-DFT, which allow the numeric generation of cubic and quartic force fields.[35] An interesting approach that uses harmonic approximation to scrutinize the most important modes and reduced dimensionality anharmonic models, has just been presented in literature.[36]

Current challenge for methods aiming at simulating electronic spectra shapes retaining a quantum mechanical (QM) description of vibrational motion is represented by flexible molecules[37](*i.e.* those characterized by one or more large amplitude, anharmonic motions) in condensed phase, in particular when significant and specific interactions with the environment (like a homogeneous medium, as a simple solvent, or a heterogeneous one, as a protein or a surface) can be established. For systems in aprotic solutions some solvent effects can be introduced in standard vibronic calculations,[38,39] computing the PES, and even the inhomogeneous broadening,[22] with implicit models like the polarizable continuum model[40] (PCM). Conversely, when strong specific interactions between the solute and its embedding medium take place, an explicit description of the environment should be taken into account.

Molecular Dynamics (MD) simulations are very well suited to explore conformational space in these situations, and their usage to simulate the electronic spectra through classical ensemble averages of vertical energies (CEA-VE) is well established.[2,41–48] In practice, in these hybrid QM/MD methods, sometimes re-

ferred as sequential classical-QM approaches,[42,49] the spectral shape arises from the distribution of transition frequencies and intensities at a representative set of conformations (or snapshots) chosen along the MD trajectory. This is an application of the so called Franck-Condon (FC) classical principle.[4] A key ingredient for the success of such approaches stands in the accuracy of the force-field (FF) underlying the MD simulations, *i.e.* on the FF's capability to reliably represent the molecule's equilibrium geometry and the corresponding harmonic frequencies, its internal flexibility and its interactions with the surrounding environment.[7,50–53] The usage of standard FFs that do not meet these requirements may, in fact, lead to wrong positions and widths of the simulated spectra.[7,53] Yet, since vibrational motions are described classically, two main limitations arise for this methodology: (*i*) it cannot reproduce vibronic peaks and (*ii*) the contribution to the spectral width is underestimated, because the classical Boltzmann distribution is narrower than what expected at quantum level. The extreme case occurs at 0 Kelvin when the classical distribution is a single structure while the quantum distribution has still a finite width, but even at room temperature the underestimation can be remarkable for high-frequency modes.[6,7,54,55] This second limitation is usually partially overcome applying to each computed transition frequency an empirical broadening. The latter is sensibly smaller than the one usually employed in a static approach (i.e. based on the minimum energy conformation only), but still of phenomenological nature.

Non-phenomenological treatments have been recently proposed, by explicitly accounting for NQEs in the MD,[55] using path integral formalisms like the ring polymer MD.[56] These very interesting approaches only introduce NQE in the initial state distribution, and therefore cannot reproduce vibronic peaks.

Moreover, they are expected to show limitations also for structureless bands

since the adoption of the true quantum initial-state distribution only guarantees the exactness of the first and second moments of the spectrum, while higher-order moments (ruling the asymmetry), as well as vibronic resolution, inevitably depend on a proper description of the quantum time-evolution on the final state PES.[4] In some cases the latter can be computed with "on-the-fly" semi-classical approximations of the propagator,[57] but these methodologies are, at the state of the art, only feasible for small systems. For larger ones, like flexible molecules in condensed phase, a number of approximated protocols to mix classical MD sampling and vibronic computations have been proposed.[7,37,48,58–62] In the simplest approaches, the vibronic spectrum of the solute has been considered independent of the specific MD snapshot.[58–61] A way to go beyond this approximation, explicitly accounting for the coupling of intra-molecular and inter-molecular vibrations, is to use in vibronic calculations spectral densities extracted from classical MD trajectories.[37,51,53,63] The potentiality of such approach has been recently illustrated by Loco et al.;[64] its partial limitation is that the spectrum is computed with reference to vibronic harmonic models that only account explicitly for linear couplings. The effects of quadratic differences in the initial and final states PES, which are responsible for shift of the maxima[5] and contribute to the spectral width,[4] are only implicitly reflected in the parameters of the spectral density. Moreover the inclusion of non-Condon effects does not appear straightforward. More recently,[37,48,65,66] Zuehlsdorff and co-workers proposed an interesting methodology to combine the ensemble approach (i.e. the sampling from a MD trajectory) with vibronic calculations, and named it E-ZTFC (Ensemble-Zero Temperature FC). In practice, a quantum vibronic spectrum of the solute is computed at 0 K and thermal fluctuations of the vertical energy and the transition dipole strength, due to intra-molecular and solvent motions, are introduced at classical level with a conformational sampling

from MD trajectories. Some effects of specific solute-solvent interaction on the vibronic spectrum are introduced by recomputing the 0K vibronic spectrum for a small (typically 5) number of different snapshots and taking the average. In ref. 66 the same authors further extended E-ZTFC methodology introducing NQE also in the conformational sampling, by performing ab initio path-integral MD. Both methods are very interesting and showed that anharmonic corrections may play a remarkable role in the spectra and be enhanced when NQEs are taken into account in the MD simulation. Nonetheless, as explained by the authors, this approach suffers of a partial double-counting of the effect of intra-molecular vibrations. The latter depends on the temperature and the frequency of the mode, and therefore its impact is system-dependent and not easily quantifiable *a priori*.

In this framework, a mixed quantum-classical (mqc) approach for the computation of electronic spectra in molecules with a set of stiff (harmonic) modes and one or few internal large-amplitude motions was recently proposed by our group.[7,62] It is based on an adiabatic approximation, which assumes that the large amplitude motion is slow compared to the stiff modes and can be therefore treated classically. In this work, we start again from this adiabatic approximation to present a general method for computing electronic spectra of flexible dyes in explicit environments without introducing, in principle, any phenomenological broadening, which describes soft modes of both solute and solvent at classical level, and the stiff modes of the dye at vibronic quantum level. Concretely, a first MD simulation with an accurate, quantum-mechanically derived FF (QMD-FF)[67–69] provides a representative set of configurations of the solute+solvent system. Reduced-dimensionality vibronic models for the stiff coordinates are then computed from energies, gradients, and Hessians of the initial and final states evaluated in the specific configuration with a QM/MM embedded scheme. For vibronic models, we

introduce a generalized Vertical Hessian (VH) model[70] (gVH), so to include also the effect of frequency changes and Duschinsky[71] mixings, and we iteratively apply proper projectors in curvilinear internal coordinates (ICs) to rigorously separate the modes to be treated at classical and quantum level, thus avoiding double-counting effects. The global spectrum eventually arises from the average, over the conformational space of the classical flexible coordinates, of configuration-specific thermally-averaged vibronic spectra. Since the here-proposed protocol combines a quantum gVH method with classical MD simulations, through an adiabatic approximation, in the following we refer to it as the $Ad-MD|gVH$ approach.

The paper is organized as follows. In Section 2 the different parts of the theoretical method and the computational protocol are explained and in Section 3 computational details are given. In Section 4 we present the results obtained on three different systems (sketched in Figure 1), where both the solute flexibility and the strength of its interaction with the solvent increase along the series: N-methyl-6-oxyquinolinium betaine (**MQ**) in water, an almost rigid system establishing H-bonds with a aqueous solvent, the flexible dithiophene (**T2**) in ethanol, and a flexible cyanidine (**Cyan**) dye which additionally has five oxydrilic groups, establishing several H-bonds in water. Finally Section 5 is devoted to discussions and conclusions.

2 Methods

2.1 Mixed Quantum-Classical spectral shape

In a TD formalism the general quantum (q) expression of the absorption lineshape $L^q(\omega)$ from the electronic state i to state$f$ is

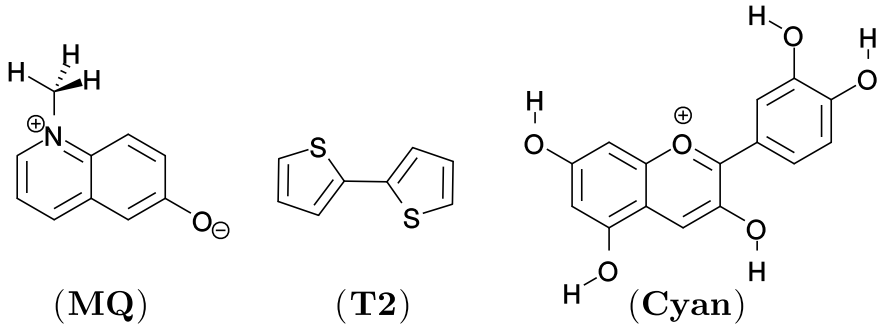

Figure 1: Molecular structure of the 3 dyes investigated in this work. (**MQ**): N-methyl-6-oxyquinolinium betaine, (**T2**): dithiophene and (**Cyan**): Cyanidin.

$$L^q(\omega) = \frac{1}{2\pi Z_{v_i}} \int \mathrm{Tr}\left[\boldsymbol{\mu}_{if} e^{-itH_f/\hbar} \boldsymbol{\mu}_{fi} e^{-(\beta - it/\hbar)H_i}\right] e^{i\omega t} dt \tag{1}$$

where Z_{v_i} is the partition function of the initial vibrational states $|\mathbf{v}_i\rangle$, Tr refers to the trace operation, $\beta = (K_B T)^{-1}$, K_B is the Boltzmann constant, T the absolute temperature, H_i and H_f are the Hamiltonians for the i and f states and $\boldsymbol{\mu}_{if}$ is their transition electric dipole moment ($\boldsymbol{\mu}_{if}$ is real and therefore equal to $\boldsymbol{\mu}_{fi}$). The absorption spectrum is $\epsilon(\omega) = C\omega L(\omega)$ where C is a constant depending on the selected units. For harmonic systems, the integrand of Eq. (1) is analytical even when frequency-changes and Duschinsky rotations exist, and also when a linear expansion of the transition dipole is considered to account for both FC and HT effects.[14–23]

According to Lax,[4] a semi-classical (sc) approximation of the spectrum lineshape, $L^{sc}(\omega)$ can be obtained expressing the trace in Eq. (1) in the coordinate representation (**Q**), and neglecting the commutators between H_i and H_f and between the operator of the nuclear kinetic energy and the transition electric dipole

moment.[4,17] We thus get

$$L^{sc}(\omega) = \int d\mathbf{Q}\rho_i^q(\mathbf{Q},T)|\boldsymbol{\mu}_{if}(\mathbf{Q})|^2 \frac{1}{2\pi}\int dt e^{i\omega t - i(H_f(\mathbf{Q})-H_i(\mathbf{Q}))t/\hbar} \tag{2}$$

where $\rho_i^q(\mathbf{Q},T)$ is the quantum coordinate distribution of the initial state at temperature T. The integral in time then collapses into a δ function and the spectral lineshape becomes

$$L^{sc}(\omega) = \int d\mathbf{Q}\rho_i^q(\mathbf{Q},T)|\boldsymbol{\mu}_{if}(\mathbf{Q})|^2 \delta\left(\omega - \Delta\Omega(\mathbf{Q})\right) \tag{3}$$

where $\Delta\Omega(\mathbf{Q}) = \hbar^{-1}\left[V_f(\mathbf{Q}) - V_i(\mathbf{Q})\right]$, and V_i and V_f are the initial and final state PESs. It is interesting to notice that Eq. (3) provides a spectral shape without vibronic resolution which, in FC approximation, exactly reproduces the first and second moment of the quantum lineshape in Eq. (1), but not higher-order momenta.[4] The integral in Eq. (3) can be evaluated from the value of the integrand at a number of structures (since now on "configurations") $\mathbf{Q}^\alpha$ with $\alpha = 1,\ldots,N_{con}$, that provide a proper sampling of the distribution $\rho_i^q(\mathbf{Q},T)$

$$L^{sc}(\omega) = \frac{1}{N_{con}}\sum_\alpha |\boldsymbol{\mu}_{if}(\mathbf{Q}^{\alpha,q})|^2 g\left(\omega - \Delta\Omega(\mathbf{Q}^{\alpha,q})\right) \tag{4}$$

where we have substituted the delta function with a convenient lineshape function g (usually a Gaussian or a Lorentzian),[41] and the superscript q on the coordinate values $\mathbf{Q}^{\alpha,q}$ reminds that the sampling is done on the quantum distribution, like, for instance, when path integral MD trajectories[55,66] are employed.

In the most popular approach, however, for sizeable systems in a solvent or in a complex environment, $\rho_i^q(\mathbf{Q},T)$ is substituted with the classical (c) distribution $\rho_i^c(\mathbf{Q},T)$ which can be sampled with a classical MD trajectory. With this new

distribution, the classical lineshape $L^c(\omega)$ is obtained according to an equation equivalent to Eq. (4):

$$L^c(\omega) = \frac{1}{N_{con}} \sum_{\alpha} |\boldsymbol{\mu}_{if}(\mathbf{Q}^{\alpha,c})|^2 g\left(\omega - \Delta\Omega(\mathbf{Q}^{\alpha,c})\right) \tag{5}$$

We now introduce a *mqc* approximation of the spectrum, which combines Eqs. (1) and (5) or (4). To this end, we consider the super system comprising the dye and its embedding. Rather than performing the standard partition into solute's and environmental coordinates, we divide all nuclear degrees of freedom (DoFs) of the whole system in two categories: the stiff modes $\mathbf{r}$, pertaining to the dye and, if needed, to some environment molecule, and the soft modes $\mathbf{R}$, represented by the flexible DoFs of the dye together with all the remaining environmental modes. The former $\mathbf{r}$ set will be handled at quantum level, while the $\mathbf{R}$ set will be treated at classical level (but semiclassical approaches are also possible). Concretely, we run a MD trajectory to sample the configurational space obtaining a representative set of snapshots ($\mathbf{R}^\alpha$,$\mathbf{r}^\alpha$) with $\alpha = 1, \ldots, N_{con}$. At this point we have all the data to obtain the classical $L^c(\omega)$ or semiclassical $L^{sc}(\omega)$ spectrum, depending on whether the MD has taken into account NQEs. In order to (re-)introduce a quantum vibronic treatment of the stiff-coordinates we invoke an adiabatic approximation, i.e. we assume that $\mathbf{R}$ coordinates are much slower than $\mathbf{r}$ ones. Therefore we can think that stiff-coordinates rearrange very quickly to any change in the position of the soft coordinates, considered frozen at each configuration α. Quadratic expansions around α of $V_i(\mathbf{r};\mathbf{R}^\alpha)$, and $V_f(\mathbf{r};\mathbf{R}^\alpha)$ allow to establish harmonic PES for both states along the stiff coordinates, and therefore compute a vibronic quantum spectrum $L_r^{\alpha,q}(\omega)$ involving these coordinates only, that is specific for $\mathbf{R}^\alpha$. To that end it is possible to use the TD expression in Eq. (1). The global spectrum

$L^{mqc}(\omega)$ can be therefore recovered as an average of all the spectra $L_r^{\alpha,q}(\omega)$.

$$L^{mqc}(\omega) = \frac{1}{N_{con}} \sum_{\alpha} L_r^{\alpha,q}(\omega) \tag{6}$$

It is interesting to notice that the expression for $L^{mqc}(\omega)$ is formally very similar to the ones for the semiclassical (Eq. 4) and classical (Eq. 5) spectra. However a fundamental difference is that the phenomenological lineshape $|\boldsymbol{\mu}_{if}(\mathbf{Q}^{\alpha})|^2 g\left(\omega - \Delta\Omega(\mathbf{Q}^{\alpha})\right)$, where g has the same shape for each snapshot, is now substituted by $L_r^{\alpha,q}(\omega)$, configuration-specific (α) quantum vibronic spectral shapes along the stiff coordinates. It is also worthy to notice that at each configuration α, a linear expansion of $\boldsymbol{\mu}_{if}$ along the stiff coordinates can be computed, and this allows for including HT quantum effects, depending on the slow coordinates also, which are lost or treated in an inaccurate way in the semi-classical and classical expressions in Eqs. (4) and (5).

2.2 Workflow of the $Ad-MD|gVH$ method

The partition in stiff and soft coordinates, pivotal for the $Ad-MD|gVH$ method, is practically achieved in two steps. First, the classical distribution of stiff and flexible coordinates is retrieved through a MD simulation performed on the target condensed phase at constant temperature and pressure. In order to ensure a consistent description of the nuclear potentials in the classical MD simulation and the quantum mechanical calculations, very accurate FFs are required, therefore specifically taylored QMD-FFs are adopted for the MD runs (Section 2.3). Next, at each representative snapshot along the MD, **R** flexible coordinates are separated from the stiff ones **r** and the contribution to the spectrum of the latter is computed quantum mechanically within a vertical harmonic model (Section 2.4).

The $Ad-MD|gVH$method is summarized in Figure 2 and can be outlined as follows:

1. Compute at QM (DFT) level for the chosen electronic state the data required for parametrization of the QMD-FFs, *i.e.* the optimized geometry, the Hessian matrix in the minimum conformation and the relaxed torsional scans of the flexible dihedrals.

2. Generate a complete FF, by combining a QMD-FF intra-molecular part with selected parameters to represent the solvent-solvent and solute-solvent interaction. The former QMD-FF for the solute is derived from the previously computed QM data using the JOYCE protocol[67–69] obtaining at once all force constants and equilibrium values for all selected stiff and flexible ICs.

3. Run a classical MD simulation at temperature $\boldsymbol{T}$ for the solute+solvent system, to get a proper sampling of the configurational distribution of all coordinates, $\rho^{c}(\mathbf{R},\mathbf{r})$.

4. Compute the Hessian matrices of the initial and final states of the solute (plus, if necessary, the most significant solvent molecules) at each configuration, including the effect of the surrounding medium with an adequate embedding scheme. At this step, if HT effects are important, also derivatives of the transition dipoles are computed.

5. Move to a set of non-redundant set of curvilinear coordinates defined in terms of all valence internal coordinates, i.e. bonds, angles and dihedrals. Soft modes are expressed in terms of such internal coordinates. Project out the soft coordinates $\mathbf{R}$ from the initial and final state Hessians at each snapshot, and use the resulting reduced dimensionality Hessians and gradients to

build up a gVH vibronic model along the stiff coordinates, specific for the considered configuration.

6. Compute the vibronic spectrum at temperature $\boldsymbol{T}$ with the TD implementation, by the $\mathcal{FC}classes$ code.[72]

7. Compute the final spectrum as the average of the vibronic spectra at each snapshot.

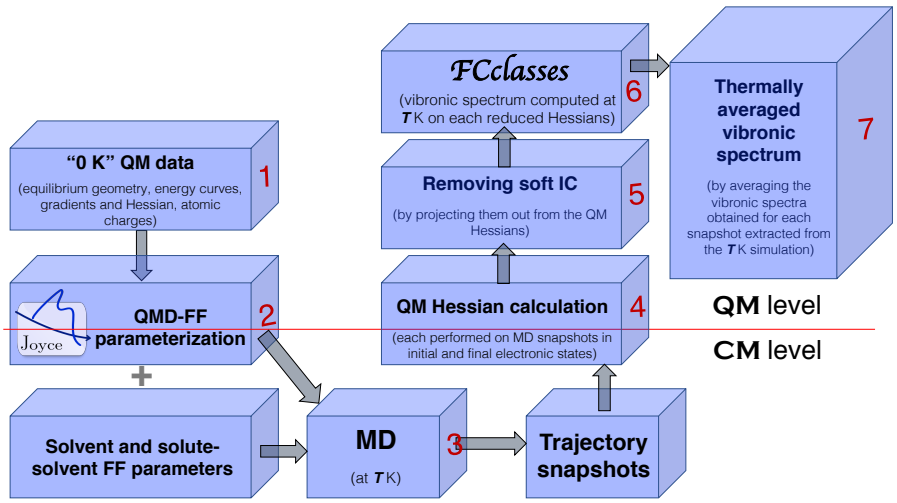

Figure 2: Workflow of the proposed $Ad-MD|gVH$method. The red line evidences the separation between the classical (CM) and quantum mechanical (QM) level of theory.

The generation of the QMD-FF and the gVH model with removal of soft ICs are crucial steps, and they are described in some detail the following sections.

2.3 QMD-FF parameterization

The parametrization of the solute's intra-molecular FF is carried out through the JOYCE protocol,[67–69] based on QM data purposely computed for the target

molecule. The following functional form is employed,

$$E^{intra}_{QMD-FF} = E_s + E_b + E_{st} + E_{ft} + E^{intra}_{Nb} \tag{7}$$

where E_s, E_b and E_{st} are the potential terms related to stretching, bending and stiff torsions, and are described by harmonic potentials. E_{ft} refers to the flexible torsions, which are described by a series of periodic (sine) functions. The last term, E^{intra}_{Nb}, contains the non-bonded intra-molecular interactions, implemented as a sum of electrostatic charge-charge and Lennard-Jones (LJ) terms.

The parameterization is carried out by minimizing the objective function I^{intra}:

$$I^{intra} = \sum_{g}^{N_{geom}} W_g \left[\Delta U_g - E^{intra}_g\right]^2 + \sum_{K\leq L}^{3N-6} W'_{KL} \left[H_{KL} - \left(\frac{\partial^2 E^{FF_{intra}}}{\partial Q_K \partial Q_L}\right)\right]^2_{g=0} \tag{8}$$

where g is a chosen molecular conformation, ΔU_g its QM internal energy, Q_K is the K^{th} normal coordinate and H_{KL} is a QM Hessian matrix evaluated in the minimum energy geometry ($g = 0$). W_g and W'_{KL} are selected weights, which are set according to the JOYCE default values.[7,50,52,53,69] Further details about the parameterization are included in Section **S2** of the Supporting Information (SI).

2.4 gVH vibronic model in reduced dimensionality spaces

The $Ad-MD|gVH$ method displayed in Figure 2 requires identifying and projecting out the molecular soft DoFs. In general, such DoFs correspond to the flexible dihedrals, as defined in the QMD-FF, but some molecules may present, in one or both states, additional flexible DoFs, like e.g. the pyramidalizations of some centers. Finally additional flexibilities may occur if some intermolecular solute-solvent modes (e.g. H-bonds) must be retained in the vibronic calculations.

Therefore, to be as general as possible, we name $\mathbf{x}$ the set of all Cartesian coordinates of any molecule for which at least one vibrational mode must be included in the vibronic model, and $\mathbf{X}$ the Cartesian coordinates of all the other solvent molecules. We work in a VH approach,[70,73] *i.e.* we build up harmonic potentials, for both i and f states, along the stiff coordinates, with a second-order Taylor expansion around the same starting geometry, α ($\mathbf{x}^\alpha$,$\mathbf{X}^\alpha$), contained in the α-th MD snapshot. However, while standard VH approaches are built from the initial-state equilibrium geometry, in general the MD configuration α will not be a minimum along the stiff-coordinates either in the initial or in the final state, and therefore the VH model needs to be generalized, to obtain what we name a gVH model.

To apply this gVH approach, we first compute, at QM level for each MD snapshot α, the energies ($V_0^{i,\alpha}$ and $V_0^{f,\alpha}$), gradients ($\mathbf{g}_x^{i,\alpha}$ and $\mathbf{g}_x^{f,\alpha}$) and Hessians ($\mathbf{H}_x^{i,\alpha}$ and $\mathbf{H}_x^{f,\alpha}$) along the coordinates $\mathbf{x}$. This is done describing the remaining molecules, with coordinates $\mathbf{X}$, with some adequate embedding scheme and considering the values of these coordinates frozen. From now on, for the sake of brevity, we will neglect the superscript α, but it will be reintroduced at the end of this section, before giving the final equations of the gVH model. The second step is to shift to internal curvilinear coordinates as (i) they provide the most natural set to define reduced-dimensionality models, since soft modes are much better described in internal coordinates than in Cartesian ones, (ii) at variance with Cartesian coordinates, they allow to rigorously remove rotational coordinates and thus properly define normal coordinates when the Hessian is not computed at a stationary point.[7]

Nonetheless, when using curvilinear internal coordinates, one needs to take into account that, except at stationary points,[74] the Hessian elements are not invariant with respect to the coordinate frame, because the metric tensor is not constant

along the conformational space. This eventually means that the computed frequencies depend on the selected set of non-redundant curvilinear internal coordinates. The non-redundant set selected in this work corresponds to linear combinations of all possible bonds, angles and dihedrals, following the recipe described by Reimers,.[75] Indeed, in a recent work,[70] we showed that such non-redundant set generally provides Hessian elements at non-stationary points consistent with those computed at nearby stationary points, in contrast to other sets such as the Z-matrix coordinates. In order to construct the non-redundant set from the redundant one, the **G** matrix corresponding to all bonds, angles and dihedrals is diagonalized, and the linear combinations correspond to the N_{vib} eigenvectors associated to non-zero eigenvalues. Yet, it might be worth noticing that other valid strategies to define non-redundant sets of internal coordinates have been proposed in literature.[76,77]

The new protocol that we introduce to remove an arbitrary number of internal coordinates generalizes what proposed by Jackels et al.[78] for a single coordinate. We first define the projector that removes a given coordinate, $\mathbf{s}$, from an arbitrary vector of the space, $\mathbf{v}$, as the following linear application,

$$P(\mathbf{v}) = \mathbf{v} - \frac{\mathbf{s}(\mathbf{s}, \mathbf{v})}{|s|^2} \tag{9}$$

where $(,)$ indicates scalar product and $|s|^2 = (\mathbf{s}, \mathbf{s})$ is the square modulus of the vector $\mathbf{s}$. In the case of non-orthogonal basis, such as our valence internal non-redundant set, the metric tensor, i.e., the list of scalar products between basis vectors, is required to compute the scalar product. A given non-orthogonal basis has an associated dual basis, each having its own metric tensor, named covariant (involving scalar products of the basis vectors) and contravariant (related to the dual basis) metric tensors. The elements of the contravariant tensor, h^{ij}, corre-

spond to the entries of the $\mathbf{G}$ matrix,[78] while those of the covariant ones, h_{ij}, correspond to its inverse, i.e., $\mathbf{G}^{-1}$. It is also convenient here to highlight that some entities in the vector space are more straightforwardly represented by either the basis or its dual. For instance, in our case, an arbitrary internal coordinate is naturally represented by the non-redundant set, while gradient of the potential energy is naturally represented in the dual basis.[79]

The elements of the matrix representation of the above linear application reads,

$$P_j^i = \delta_j^i - \frac{s^i s_j}{|s|^2} = \delta_j^i - \frac{s^i \sum_k s^k h_{jk}}{|s|^2} = \delta_j^i - \frac{s_j \sum_k s_k h^{ik}}{|s|^2} \tag{10}$$

where P_j^i represents a 1-covariant, 1-contravariant tensor (in practice, a matrix element with i running over rows and j over columns), δ_j^i is the 1-covariant, 1-contravariant version of the Kronecker delta and we have explicitely given the expression in terms of either contravariant vectors (e.g., an arbitrary internal coordinate) or covariant ones (e.g., the gradient). The projector defined in terms of contravariant vectors can be written in matrix form as,

$$\mathbf{P} = \mathbf{1} - \frac{\mathbf{s}\mathbf{s}^t}{\mathbf{s}^t\mathbf{h}\mathbf{s}}\mathbf{h} \tag{11}$$

where $\mathbf{s}$ are column vectors containing the contravariant components (s^i) and $\mathbf{h}$ is a matrix containing the elements of the covariant metric tensor (h_{ij}). A similar expression is obtained in terms of covariant vectors.[78] The Hessian elements transform as a 2-covariant tensor,[79] and thus the application of the projector over the Hessian, $\mathbf{H}$, can be expressed as,

$$\widetilde{\mathbf{H}} = \mathbf{P}^t\mathbf{H}\mathbf{P} \tag{12}$$

In order to run the process iteratively one must also update the metric tensor

and the remaining vectors to be projected out. The former tranforms as $\widetilde{\mathbf{h}} = \mathbf{P}^t\mathbf{h}\mathbf{P}$, while the latter are updated by directly applying the projector over them, $\widetilde{\mathbf{s}}_j = \mathbf{P}\mathbf{s}_j$. At this point, we are ready to project the next coordinate. This iterative protocol is summarized in the scheme of Figure 3. We notice that we already proposed an approximate version of this protocol in ref.[80] which worked satisfactorily only to remove torsions, because they are rather orthogonal to the rest of coordinates.

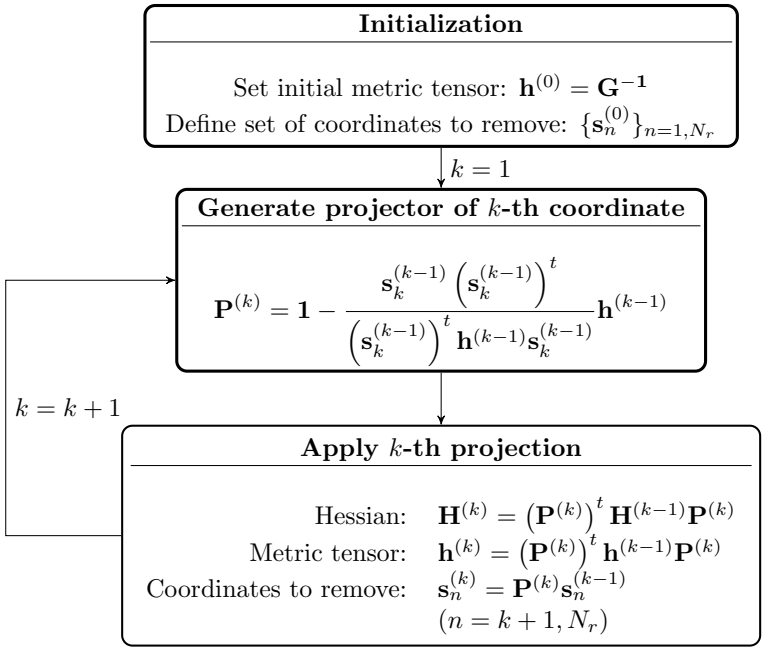

Figure 3: Summary of the iterative method to remove a set of N_r coordinates. The superscripts in parenthesis indicate the iteration to which the element corresponds. The loop is repeated while $k \leq Nr$

After all the soft coordinates have been eliminated, the gradient, $\mathbf{g}_r$, and Hessian, $\mathbf{H}_r$ are contained in the reduced space of the $\mathbf{r}$ stiff coordinates only. We can therefore straightforwardly write down quadratic expansions along the $\mathbf{r}$ stiff coordinates for the PES of state k

$$V^{k,\alpha}(\mathbf{r}) = V_0^{k,\alpha} + (\mathbf{g}_r^{k,\alpha})^T(\mathbf{r} - \mathbf{r}^\alpha) + (\mathbf{r} - \mathbf{r}^\alpha)^T\mathbf{H}_r^{k,\alpha}(\mathbf{r} - \mathbf{r}^\alpha) \tag{13}$$

where we reintroduced the superscript α to make explicit the dependence of this

expansion on the specific configuration α, characterized by the flexible set $\mathbf{R}^\alpha$. $V_0^{k,\alpha}$ is the energy of PES $V^{k,\alpha}(\mathbf{r})$ at the snapshot geometry α, while its minimum is at $\mathbf{r}_0^{k,\alpha} = \mathbf{r}^\alpha - (\mathbf{H}_r^{k,\alpha})^{-1}\mathbf{g}_r^{k,\alpha}$, with energy $V_{min}^{k,\alpha}$, simply obtained by substitution in Eq. 13.

Finally, application of the Wilson's GF method[81,82] leads to the definition of effective normal coordinates $\mathbf{Q}^{k,\alpha}$ for both states

$$\mathbf{r} - \mathbf{r}_0^{k,\alpha} = \mathbf{L}^{k,\alpha}\mathbf{Q}^{k,\alpha} \tag{14}$$

with normal frequencies $\mathbf{\Omega}^{k,\alpha}$. We can therefore establish a Duschinsky relation between $\mathbf{Q}^{i,\alpha}$ and $\mathbf{Q}^{f,\alpha}$

$$\mathbf{Q}^{i,\alpha} = \mathbf{J}^\alpha\mathbf{Q}^{f,\alpha} + \mathbf{K}^\alpha \tag{15}$$

$$\mathbf{J}^\alpha = (\mathbf{L}^{i,\alpha})^{-1}\mathbf{L}^{f,\alpha} \tag{16}$$

$$\mathbf{K}^\alpha = (\mathbf{L}^{i,\alpha})^{-1}(\mathbf{r}_0^{f,\alpha} - \mathbf{r}_0^{i,\alpha}) \tag{17}$$

where $\mathbf{K}^\alpha$ is the displacement vector between the equilibrium positions along the stiff-coordinates in the two states, and the Duschinsky matrix $\mathbf{J}^\alpha$ is orthogonal because the $\mathbf{G}_r$ matrix has been defined at the same geometry ($\mathbf{r}^\alpha$) for both states. The Duschinsky relation in Eq. (15), together with the normal frequencies $\mathbf{\Omega}^{i,\alpha}$ and $\mathbf{\Omega}^{f,\alpha}$, and with the extrapolated adiabatic energy difference $\Delta E^\alpha = V_{min}^{i,\alpha} - V_{min}^{f,\alpha}$ are the final result of the gVH model and allow to compute the vibronic spectrum $L_r^{\alpha,q}(\omega)$, which is specific for the snapshot α. This is done at the required temperature by applying the expression in Eq. (1), i.e. with standard TD techniques for harmonic systems.

It is worth stressing that although the soft coordinates are not directly included in the quantum vibronic treatment, their dynamics is still accounted for by the $Ad-MD|gVH$ method, but at a classical level. In fact, the effect of the fluctuations of the soft coordinates is reflected in the values of: (i) the adiabatic energy difference ΔE^{α}, which introduces a shift of $L_r^{\alpha,q}(\omega)$ on the energy axis that is specific for each configuration, (ii) the matrices of the normal frequencies $\mathbf{\Omega}^{i,\alpha}$ and $\mathbf{\Omega}^{f,\alpha}$, which introduce a further configuration-specific fluctuation of the 0-0 transition frequency and, finally, (iii) the $\mathbf{K}^{\alpha}$ vector and $\mathbf{J}^{\alpha}$ matrices that, together with normal frequencies, rule the spectral shape of $L_r^{\alpha,q}(\omega)$.

2.5 Final remarks on the method

The *mqc* expression for the $Ad-MD|gVH$ spectrum was obtained on the grounds of an adiabatic hypothesis. In refs. 7,62 we adopted an analogous hypothesis to formulate the expression for a *mqc* spectrum for a molecule with one or few soft internal coordinates. In those cases however, the conformational integral was performed on a grid of equally spaced points along the soft coordinates with weights that, we showed, depend on the free energy. This grid approach is not suitable for large systems in an environment, where the soft (large amplitude and slow) modes are numerous since they include both solute and solvent modes. Therefore it was necessary to devise a new approach able to accommodate the possibility to perform the conformational integral on the grounds of an effective MD simulation.

In practice in our method we move to the "classical set" $\mathbf{R}$ all flexible modes. The accuracy of this approximation is expected to be better the slower these motions are. This assumption is tested with simple models in section **S1** of the SI, and the conclusions are briefly summarized at the beginning of the Results section herein. Since each snapshot taken from the MD represents, by definition, a

configuration out of equilibrium, nothing guarantees in principle that the harmonic expansion in Eq. 13 give rises to all positive frequencies, i.e. represents effective fast modes **r** with stable oscillations around an equilibrium position on both the initial and final states of the electronic transition. However, this is of course a requirement for the computation of the vibronic spectrum $L_r^{\alpha,q}(\omega)$. Therefore, as shown in the Results section, a pre-screening of the expected robustness of our $Ad-MD|gVH$ prediction for the spectra is performed analysing the occurrence of imaginary frequencies and if they are reduced by moving one or more soft coordinates to the "classical set". While sporadic problematic snapshots are clearly statistically irrelevant, a large fraction of snapshots with imaginary frequencies along stiff modes would indicate either the non applicability of the method or that additional DoFs should be considered "soft" and moved to the **R** set.

Starting from the same adiabatic hypothesis we made in refs. 7,62, Zuehlsdorff et al. reported very recently, in the SI of ref. 66, an expression for the calculation of the spectrum of a solute in a solvent very similar to the one we gave in Eq. (6). Some significant formal differences however exist, that make our $Ad-MD|gVH$ method of more general applicability. The expression of Zuehlsdorff and co-workers is suitable for the standard partition that identifies the stiff coordinates with the solute and the soft coordinates with the solvent ones, whereas, thanks to the adoption of suitable projectors, in our approach soft and stiff modes can be chosen among all the degrees of freedom of the solute+solvent system (although clearly, most of the solvent coordinates will always be in the classical set). A second more technical difference, but pivotal to the generalization we just mentioned concerns with the PES expansion around the selected conformation. Zuehlsdorff and co-workers compute the harmonic PES according to an Adiabatic Hessian (AH) model, i.e. in a given configuration they locate the equilibrium ge-

ometry of both the initial and final states PESs and expand them quadratically around their own minima.[73] Although our approach may recast also in an AH framework, we chose a VH model because it straightforwardly allow us to include in both soft and stiff subsets either solute or solvent coordinates. It is much more complicated to allow such a possibility within a AH approach, because it would be necessary to perform constrained optimizations freezing simultaneously a number of internal coordinates (or their combination) of the solute, and the solvent (Cartesian) coordinates. To the best of our knowledge this is not doable in most of the popular quantum chemistry codes.

Apart from these formal differences, in practice Zuehlsdorff et al. did not compute spectra according to the proposed expression mainly because of the computational cost. We overcame this technical problem by exploiting in vibronic calculations, the very fast and effective TD methodology implemented in our code $\mathcal{FC}classes$. As a matter of fact a calculation of $L_r^{\alpha,q}(\omega)$ typically requires seconds on a single-core of a standard machine.

3 Computational details

The whole $Ad-MD|gVH$ computational protocol is based on a combination of four different codes, namely the GAUSSIAN16 package for electronic calculations,[83] the GROMACS engine[84,85] for MD simulations, and two programs written by some of the authors of this contribution:, the JOYCE program,[86] for the generation of the FFs, and version 3.0 of the $\mathcal{FC}classes$ code,[72,87] for the computation of the vibronic spectra. Details are given in the following subsections.

3.1 QM calculations

All QM calculations have been performed at DFT level for the ground electronic state and TDDFT for the excited states using the GAUSSIAN16 package.[83] The level of theory was chosen based on previous works, namely PBE0/6-31+G(d,p) for **MQ**,[6] PBE0/6-31G(d) for **T2**,[88] and CAM-B3LYP/6-311+G(d,p) for **Cyan**.[52] The DFT database necessary for QMD-FF parametrization includes a full geometry optimization in the desired electronic state, the Hessian computed at the equilibrium geometry and a number of relaxed energy scans along the flexible torsions. In all cases, the data are computed with the same level of theory employed to build the model harmonic PESs for vibronic calculations.

3.2 Force-fields

Specific FFs were here parametrized for two of the three investigated systems (**MQ** and **T2**), while the FF **Cyan** was taken from previous work of some of us.[52]

All three FFs were built as detailed in the following. The intra-molecular parameters of the dyes (solutes) were carried out with the JOYCE program,[67–69] according to the procedure briefly discussed in the previous section and detailed in the SI. The solute's atomic charges, entering the expression of the solute-solvent inter-molecular term (see equations (22) and (23) in the SI), were obtained from QM calculations through either the CM5 (for **MQ** and **T2**)[89] or the RESP (for **Cyan**)[90] procedure, applied on the optimized geometry of the target solute, while accounting for the solvent through the PCM model.[40] It might be worth noticing that, as discussed in some detail in section S3.5 of the SI, the adoption of a different scheme (i.e. RESP rather than CM5) for retrieving specific point charges for **Cyan** was dictated by the fact that this species is charged, hence the reliability of the Hirsfield scheme, from which CM5 charges are derived,[89] is not ensured.[91] All other

parameters specifying the solvent intra-molecular term (see equations (15)-(21) in the SI) and the solute-solvent and solvent-solvent inter-molecular contributions (*i.e.* solute and solvent inter-molecular LJ parameters and solvent point charges (see equation (23) in the SI) were transferred from the OPLS FF.[92–94] A complete list of the FF parameters for all systems and further details on the parameterization procedure can be found in Section **S2** of the SI.

3.3 MD simulations

All MD simulations, as well as molecular mechanics (MM) optimizations, were performed with the GROMACS engine,[84,85] in the NPT ensemble, on systems composed of one solute molecule (**MQ**, **T2** or **Cyan**) and a large number (~ 1000) of solvent molecules (either water or ethanol). In the case of **Cyan**, a Cl^- counter ion was also added,[52] to ensure electroneutrality. For each dye, two different schemes were applied, to investigate on the effect of including or not including the fast stretching vibrations in the MD runs. To this end, each run was separately carried out without or with the LINCS algorithm,[95] to constrain all bond lengths to their equilibrium value. In the former case the employed time step was 0.2 fs, whereas, without accounting for the fast stretching motions, the time step was increased to 1 fs. In all runs, temperature T (300 K) and pressure P (1 atm) were kept constant through the v-rescale[96] and Parrinello-Rahaman[97] schemes, using coupling constants of 0.1 ps and 1 ps, respectively. A cutoff radius of 11 Å was employed for both short-range charge-charge and LJ terms, whereas long-range electrostatics was accounted for through the particle mesh Ewald (PME) procedure. All systems were first minimized, and afterwards atomic velocities were assigned according to a Maxwell–Boltzmann distribution at 300 K. Each system was first equilibrated for 2 ns; thereafter, production runs were performed

for further 6 (**MQ**, **T2**) or 3 ns (**Cyan**).

3.4 QM:MM gradient and frequency calculations

Along the MD trajectories, snapshots were extracted every 30 ps, which ensured uncorrelated conformations. An ONIOM QM:MM model was built to evaluate the energy, gradient and Hessian over the solute atoms. The solute was included in the model system (high layer) while the real system was extended to include the first solvent layer. The extension of such first neighbour shell, quantified through the shell radius R_{cut}, was assessed, as detailed in the SI (see Figures (S11)-(S15)), based on the solvation structure retrieved from the MD runs: for all dyes, R_{cut} was fixed at 4 Å.

Within the QM:MM ONIOM scheme, the model system is treated at DFT and TDDFT level, adopting the same functional and basis already adopted to generate the QM data to parametrize the QMD-FF, and the real system is handled at the same MM potential used in the MD simulations. Finally, the ONIOM calculation was carried out by taking into account also all the remaining solvent molecules, within a radius of 40 Å from the center of gravity of the solute, according to an electronic embedding (EE) scheme, where all solvent atoms are treated as point charges. It is worth mentioning that using the simple EE scheme also to treat the first solvation shell (i.e. neglecting Lennard-Jones interactions) may lead to the occurrence of a large number of spurious imaginary frequencies, as reported in Section **S4.2** of the SI. Although here we focus on FC transitions, we recall that computation of TD-DFT analytical excited-state Hessians with Gaussian16 package also provides, at no additional cost, the derivatives of the transition dipoles, so that $Ad-MD|gVH$ calculations including HT effects do not require in principle additional cost. Some further testing is however necessary to set the most proper

embedding scheme to obtain such derivatives.

3.5 Vibronic calculations

The vibronic computations have been performed with the version 3.0 of the $\mathcal{FC}classes$. For each snapshot it reads energies, gradients and Hessians of the initial and final electronic states computed by GAUSSIAN16, projects out the soft modes, builds up the reduced dimensionality gVH model and computes the vibronic spectrum with the TD approach[22] at 300 K. For the electric transition dipole we adopted the FC approximation. We note that Eq. 6 accounts for the whole lineshape, without requiring the adoption of any phenomenological broadening. However, since the sum over conformations, α, is necessarily finite, the average arising from Eq. 6 may display significant noise. Therefore, in order to smooth the final plots, compensating the limited conformational sampling, all individual lineshapes, $L_r^{\alpha,q}(\omega)$, are convoluted with a narrow a Gaussian with HWHM=0.01 eV. In section S5 of the SI, we show that such procedure does not change the overall spectral width.

4 Results

4.1 Simple harmonic models

In Section S1 of the SI, the proposed mqc method is compared with classical (c) approximation for a model harmonic system for which the exact quantum vibronic calculation is possible. In this case the MD run is not necessary since the classical (Boltzmann) distribution is known and analytical. It is shown that $Ad-MD|gVH$ approach largely outperforms the c one, both in terms of shape and position of the spectra. When soft modes have a frequency $\leq$ than the thermal quantum ~ 208 cm^{-1}, the $Ad-MD|gVH$ spectrum is practically exact, if soft

and stiff modes are not coupled or moderately coupled. At lower resolutions, even higher-frequency modes could be included in the set of the classical modes without a deterioration of the results. Finally, the robustness of the method is tested by including in the model an artificial very strong coupling between quantum modes and the ones with frequencies lower than 200 cm^{-1}, included in the classical set: even in this case, low- and intermediate-resolution $Ad-MD|gVH$ spectra are still fairly good, while high-resolution vibronic progressions can manifest inaccuracies.

4.2 Flexible dyes in solution

In this section the $Ad-MD|gVH$ approach is applied to simulate the electronic spectra of the 3 dyes sketched in Figure 1. **MQ** is a rather rigid fused cycle

Table 1: Number of snapshots extracted along the dynamics of the different dyes exhibiting imaginary frequencies. The normal mode analysis is performed in the full dimensionality space (Full) or in two different reduced dimensionality spaces, either projecting out only the flexible torsions (rmTors) or also removing selected pyramidalizations (rm[Tors+Pyr]). The label in parenthesis defining the MD run in the second column refers to MD runs where the solute either has unconstrained (U) or constrained (C) bonds or is treated as a rigid rotor (R).

Calculations Settings			Full		rmTors		rm[Tors+Pyr]	
System	MD	Nsnap	S0	S1	S0	S1	S0	S1
MQ@H2O	S0(U)	200	31	50	2	6	0	0
MQ@H2O	S0(C)	200	20	40	0	1	0	0
MQ@H2O	S0(R)	200	1	4	0	1	0	0
T2@EtOH	S0(C)	200	0	11	0	7	0	5
T2@EtOH	S1cis(C)	200	14	23	0	22	0	0
T2@EtOH	S1trans(C)	200	1	1	0	1	0	0
Cyan@H2O	S0(U)	100	11	22	0	6	0	3

which establishes specific H-bonds with the water solvent. It also features a easily-rotating methyl group, which, however, is not expected to have a relevant role in the spectra. **T2** is conversely characterized by an inter-ring torsion whose flexibility is markedly different in the ground (S0) and in the excited (S1) state. It has been suggested that this feature has a large and different impact on absorption and

emission spectra.[88] Hence, due to the possibility that the intramolecular flexibility breaks the **T2** absorption/emission mirror symmetry, we also simulate the emission spectrum, exploiting the JOYCE's capability to deliver QMD-FF also for electronic excited states.[50,98] Finally, **Cyan** is a more complex dye, characterized by a flexible torsion that tunes the coplanarity between the phenyl and naphtyl rings and several rotatable hydroxyl groups, capable of strong interactions with the surrounding solvent molecules. For all of these systems, we simulate the absorption spectra. In all cases, the spectra are computed in different solvents, for which experimental data are available: water for **MQ** and **Cyan**, ethanol for **T2**.

4.2.1 N-methyl-6-oxyquinolinium betaine

We start focusing on **MQ** in water, including all solvent's DoFs in the classical set. Given its overall stiffness, **MQ** constitutes a relatively simple system to benchmark our methodology. In fact, the QMD-FF parameterization is carried out by assigning a harmonic potential to each internal coordinate except the flexible dihedral involved in the rotation of the methyl group around the N–CH_3 bond (Figure 1). The JOYCE parameterization was carried out with a final standard deviation of $7 \cdot 10^{-3}$ kJ/mol, obtaining the best-fit parameters reported in detail in the SI (Section 2.3). In Figure 4 the overall quality of the QMD-FF is shown through the comparison of the FF frequencies and torsional relaxed energy scans obtained for the methyl rotation with their QM counterparts. Vibrational frequencies are perfectly reproduced, and the overlap of MM and QM modes is generally significant. Moreover, the torsional profile provided by the QMD-FF remarkably improves over the standard GAFF one. Methyl rotation is also the slow DoF projected out of the vibrational space adopted to define the effective normal modes, and is defined as the linear combination of the six dihedrals with N–CH_3 bond in

the center (see definition (24) in the SI). Preliminary analysis revealed that the pyramidalization of the nitrogen atom contributes to the flexibility in the system, at least on the S1 state. The projection of complex DoFs, such as pyramidalizations, is not straightforward. In this case, we found that the most appropriate way to define this coordinate ζ in the projector was the combination of 2 dihedral angles (equation (25) in the SI).

The MD simulations that provide the conformational sampling of the system were carried out with different approaches as far as the fastest vibrations in the system are concerned. The bond lengths and angles of all water molecules were always constrained to their equilibrium values with the SETTLE[99] algorithm, in compli-

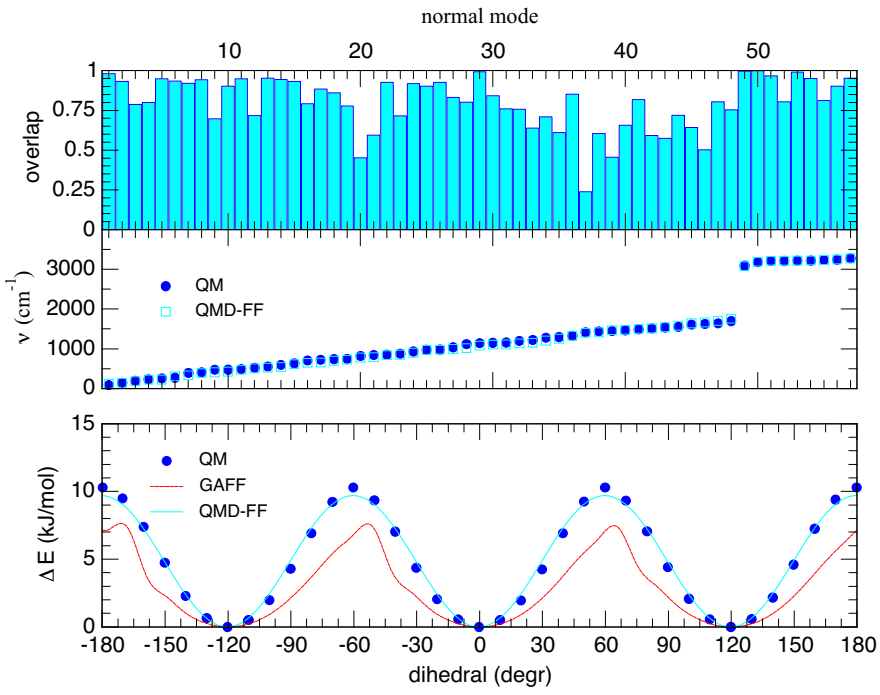

Figure 4: Top panel: overlap between the QM and the QMD-FF normal modes. Middle panel: comparison between the vibrational frequencies ν computed at QM level (solid circles) and through the QMD-FF (empty squares). Bottom panel: torsional energy profiles for the δ dihedral computed at QM and QMD-FF level.

ance with the standard TIP3P model adopted. As far as the solute is concerned, we tested three different approaches: (a) all its DoFs were left unconstrained, (b) all bonds were constrained with the LINCS algorithm[95] or (c) it was treated as a moving rigid rotor. In model (c), in analogy with the approach we presented in ref. 27, we applied a stiff harmonic potential to all DoFs, further replacing the structure by the equilibrium one at each extracted snapshot.

According to the discussion reported in Section 2.5, we start reporting in Table 1 a summary of the number of conformations where the normal mode analysis, either in S0 or S1 states, lead to any imaginary frequencies, before (Full) or after projecting out only the torsion (rmTors) or the torsion and the pyramidalization coordinate (rm[Tors+Pyr]). As expected, normal mode analysis within the Full space leads to a significant number of imaginary frequencies indicating that, despite its apparent stiffness, the molecule is characterized by some soft modes. Most of the imaginary frequencies are actually connected with the methyl torsion, and in fact, they disappear projecting this torsion out. The remaining imaginary frequencies disappear when the pyramidalization is also removed from the space, indicating that, in those (very few) snapshots, this coordinate displays a marked anharmonic behavior. Comparing the results obtained with constrained and unconstrained simulations, a larger number of imaginary frequencies are observed for the latter case (in both Full and rmTors schemes), indicating that the molecule visited more critical conformations, due to the fact that also the bond lengths are now varying along the MD samplings. Conversely, for the rigid body simulation, where the solute's structure is kept at the QM minimum, a very small number of imaginary frequencies was found, already for the vibrational analysis in the Full space. Yet, the appearance of these few imaginary frequencies indicates that the interaction with the explicit solvent particles, whose distributions changes at each snapshot,

can remarkably perturb the most flexible DoFs of the system. Indeed, when both the torsion and the pyramidalization are projected out the imaginary frequencies vanish. Such results implies a coupling between solvent and solute DoFs that is taken in account in our $Ad-MD|gVH$ method, within the limits of the accuracy of the adiabatic hypothesis.

Based on the above results, to compute the absorption spectrum, we adopt the reduced spaces (either rmTors or rm[Tors+Pyr]) to apply the $Ad-MD|gVH$ protocol in combination with either unconstrained or constrained simulations. In the case of the rigid body trajectory, the vibronic spectra are computed with the Full space since none of the internal DoFs are sampled. In all the cases, the snapshots with imaginary frequencies are discarded from the averages. Figure 5 displays the absorption lineshape simulated with all these different settings, and the characteristic parameters that describe the lineshape are summarized in Table 2.

Table 2: First moment ($\mathcal{M}_1$), standard deviation (σ) and full width at half maximum (FWHM) of the lineshapes included in Figure 5. All quantities in eV.

Sampling	VibSpace	$\mathcal{M}_1$	σ	FWHM
Unconstrained	rmTors	2.66	0.220	0.498
Unconstrained	rm[Tors+Pyr]	2.66	0.219	0.497
Constrained	rmTors	2.63	0.215	0.481
Constrained	rm[Tors+Pyr]	2.63	0.214	0.480
Rigid	Full	2.62	0.210	0.465
Rigid	rmTors	2.62	0.210	0.464
Rigid	rm[Tors+Pyr]	2.62	0.209	0.460

As observed in the figure, the unconstrained and constrained samplings lead to very similar lineshapes, with the latter giving rise to slightly narrower and red-shifted bands. The narrowing and red-shifting are even more pronounced when treating the molecule as a rigid rotor (Table 2). This effect can be connected to the different sampling of modes with large displacement, namely the C–C stretching.

The effect of the usage of different vibrational spaces is minor. The similarity of the results obtained with these three strategies is not unexpected, because in this case the solute's DoFs most relevant for the spectral shape are the stiff ones, which are well described within the harmonic approximation, whereas the soft solute's modes have only a minor effect.

In Figure 6, the lineshapes obtained from the three simulations within the rm[Tors+Pyr] space (and with the full space for the rigid sampling) are compared with experiment. All the three computational strategies provide a similar spectral shape which is in very nice agreement with experiment. The moderate changes obtained with the $Ad-MD|gVH$ method with respect to the rigid sampling improve

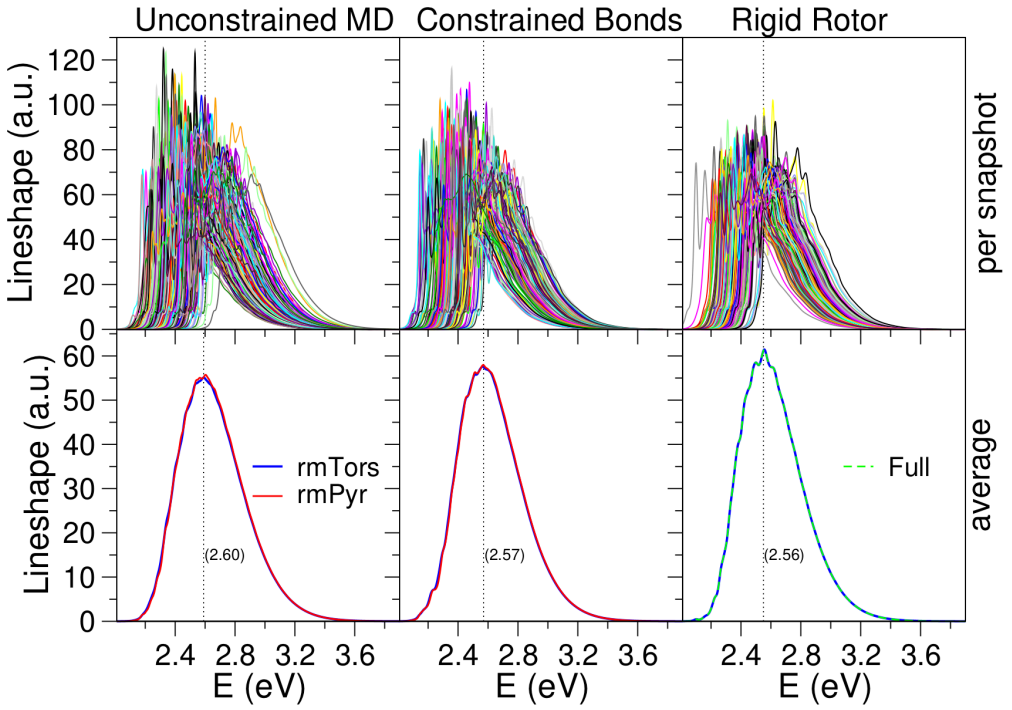

Figure 5: Absorption lineshape computed for **MQ** with the $Ad-MD|gVH$ approach presented in this work, using the different projection schemes described in the text (i.e. Full, rmTors or rm[Tors+Pyr]) over the snapshot sets extracted from the three MD runs (from left to right, unconstrained MD, constrained bonds and rigid rotor. Top panels include the vibronic spectra computed for each individual snapshot while the averages are presented in the bottom panels. The numbers in parenthesis indicate the position of the maximum, evidenced by a dotted line.

the agreement with experiment and the unconstrained simulation performs slightly better than the constrained one. Finally, the $Ad-MD|gVH$ method drastically

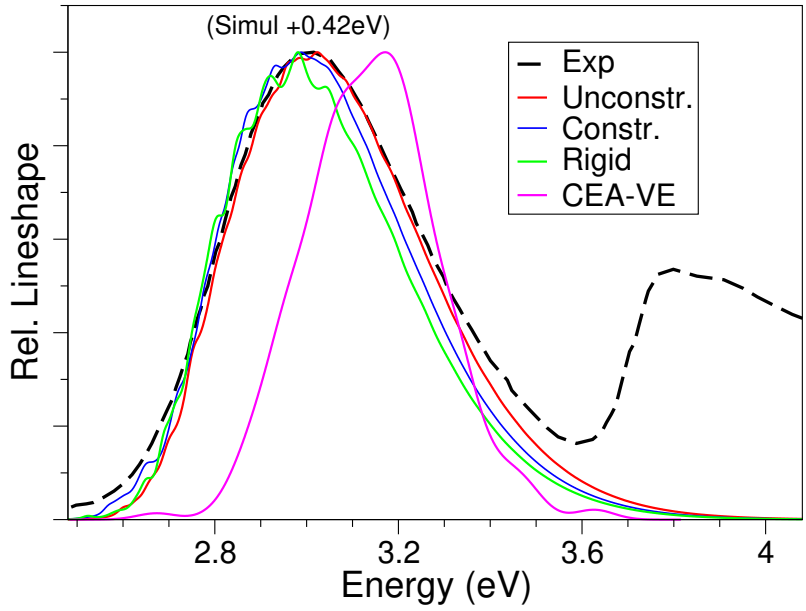

Figure 6: Absorption lineshape computed for **MQ** with the $Ad-MD|gVH$ approach presented in this work, using the different sets of internal coordinates described in the text. The standard CEA-VE spectrum is also shown, broadened with a phenomenological Gaussian curve with HWHM=0.05 eV.

improves over the CEA-VE standard approach, which is also displayed in Figure 6. In fact the spectrum obtained from the ensemble of the vertical excitations of the same snapshots used in the $Ad-MD|gVH$ method, simply broadened with a phenomenological Gaussian shape with HWHM=0.05 eV, is blue-shifted and fails in reproducing the asymmetry of the high energy wing and consequently also predict a remarkably narrower spectrum.

4.3 Di-thiophene

At variance with **MQ**, where most of the flexibility involves the methyl rotation that is not affected by the electronic transition, in **T2** two rather stiff aromatic rings are connected by a rotatable bond (C1–C1, see Figure S9 in the SI) and the

energy profile associated to such torsion changes drastically from S0 to S1. In fact, as displayed in Figure 7, the molecule is not planar in its ground-state and it is characterized by 4 minima at $\sim \pm 30°$ and $\sim \pm 150°$, connected by relatively low barriers. On the contrary, since in S1 inter-ring conjugation increases, only two planar *cis* and *trans* minima exist and are separated by a very large barrier.

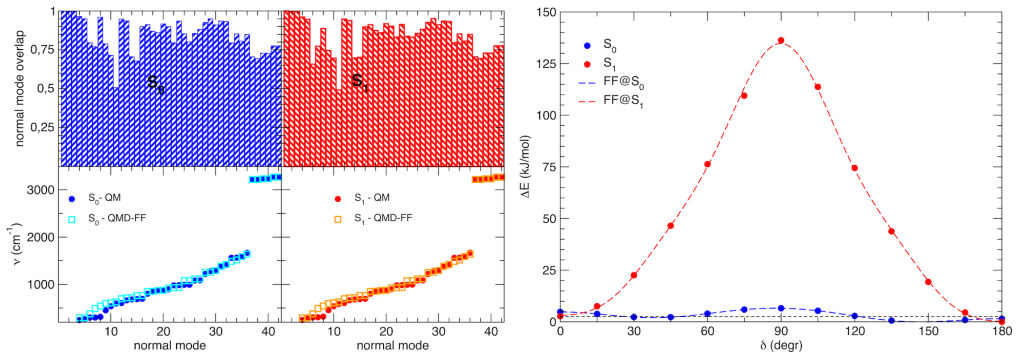

Figure 7: Left panel: QM vs FF computed vibrational frequencies; all vibrational frequencies for S0 (left) and S1 (right) are displayed (bottom) for QM (solid circles) and FF (empty squares), while the overlap between the QM and the FF normal modes (top) is displayed as a histogram. Right panel:QM vs FF computed energy torsional profiles for the δ dihedral for both states

The QMD-FFs parametrized for S0 and S1 states describe the aforementioned torsion with periodic potential terms. Both ground and excited state parameterizations were performed with the same choice of redundant internal coordinates. Beside the flexible torsion δ, it includes all possible bond lengths and angles, the "stiff" dihedrals, which rule the planarity of each aromatic ring, and the "star-like" (see Figure S9 in the SI) dihedrals governing the out-of-plane H vibrations. The final standard deviation was $8{\cdot}10^{-3}$ and $2{\cdot}10^{-1}$ kJ/mol, for S0 and S1 respectively. The analysis of the vibrational frequencies computed though the MM Hessian and at QM level is shown in the left panel of Figure 7, while in the right panel the QM vs MM torsional profiles are displayed. It appears that the flexible torsion δ tunes the coplanarity of the two rings with remarkably different energy profiles in the ground and excited electronic states. As a consequence, this rotation has a

notable impact on both the absorption and emission spectra, as indicated by the dependence of vertical energy and oscillator strength on δ (Figure S10 of the SI).

Therefore in the following we simulate both the spectra in ethanol, exploiting the fact that our $Ad-MD|gVH$ protocol is general and can be applied on equal foot to absorption and emission processes. The only difference is the state (i.e. the QMD-FF) on which the initial classical MD is performed. Since for **T2** and ethanol no strong specific solute-solvent interaction is expected, for computational convenience we run the MD constraining the **T2** stretching modes with LINCS.[95] MD simulations in S0 easily overcome the barrier along δ, which ensured a proper sampling of this coordinate. By integrating along the MD trajectory the distribution obtained for the inter-ring torsion, we found that in S0 the ratio between the populations of *trans* and *cis* is 4:1. In S1, however, the interconversion between the *trans* and *cis* isomers is not viable at room temperature, and we thus conducted one simulation per conformer, labelled as S1cis and S1trans, respectively. In this context it is worthy to notice that actually the S1 PES in the region of the *cis* side of the high barrier is made rather complicated by accessible photochemical pathways that can lead to the opening of the ring.[100]

In order to generate the reduced space to compute the vibronic contributions, we project out the inter-ring torsion δ (see expression (26) in the SI for definition). Also in this case, the pyramidalization of the carbon atoms involved in the C–C bond linking the two thiophene groups can be flexible enough to challenge the model harmonic PESs used in the vibronic calculation, and it can be more convenient to remove them from the corresponding coordinate space. Concretely, we remove the aforementioned pyramidalizations, by projecting out the improper dihedrals ζ_1 and ζ_2, as defined in equation (27) of the SI. The normal mode analysis for **T2** for snapshots along S0 and S1 trajectories, included in Table 1, shows the

existence of a non-negligible number of imaginary frequencies occurring even when the δ torsion is removed, mostly for structures obtained with the S1cis sampling. Interestingly, when the ζ_1 and ζ_2 pyramidalization coordinates are also projected out, most of those imaginary frequencies vanish. On these grounds, the emission lineshapes are computed adopting the rm[Tors+Pyr] reduced dimensionality space along the S1trans and S1cis samplings. For consistency, the same vibrational space rm[Tors+Pyr] is used to simulate the absorption lineshape from the S0 sampling.

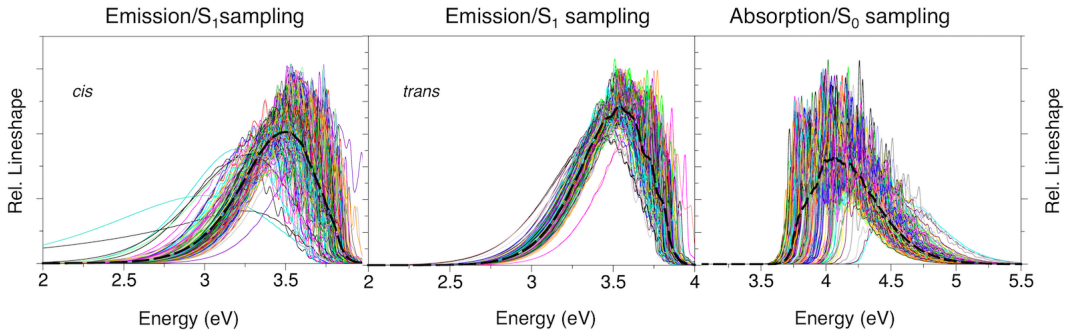

Figure 8: Vibronic spectra computed for each individual snapshot along **T2** MD trajectories of the solvated dye in its ground (right panel) or excited in *cis* and *trans* conformation, left and middle panel, respectively. The averaged spectrum is also plotted with a black dashed line.

In Figure 8 we report the vibronic spectra computed for all snapshots and their average. It can be noticed that the resulting spectra are different for position and shape. Differences are less marked in the emission from S1 *trans*. S1 *cis* show some very broad spectra, too few to have substantial statistical effect and likely connected with configurations where the PES is very anharmonic due to the nearby existence of the ring-opening pathways.[100] For absorption we do not notice such large differences in the shape of the spectra. However, due to the flat shape of the PES (see Figure 7) inter-ring torsion may acquire remarkable deviations from the minima toward 90 degrees and, due to the steepness of the S1 PES, these configurations correspond to spectra significantly blueshifted. This phenomenon

makes absorption spectrum broader than emission (see below).

In Figure 9, we compare the results provided by our protocol with the experimental ones at room temperature. Emission spectra in ethanol were taken from ref.

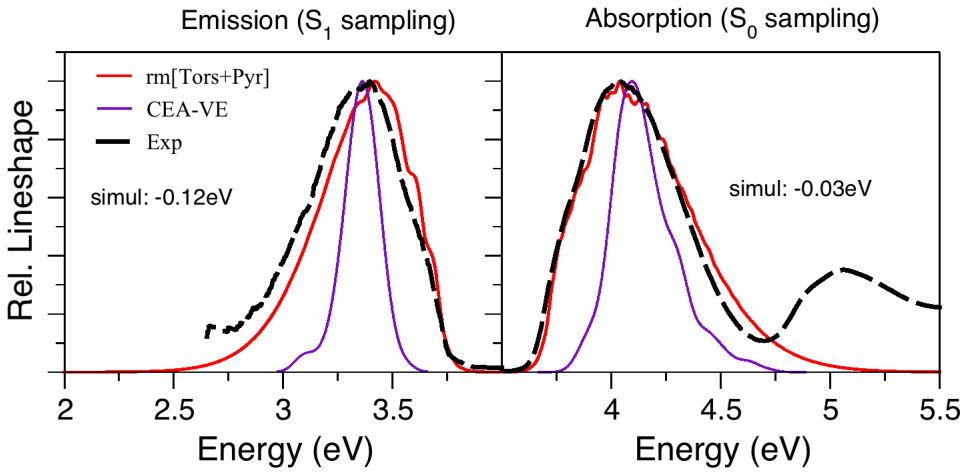

Figure 9: Absorption and emission spectra simulated with the $Ad-MD|gVH$ and the CEA-VE approaches. In the latter method, the individual VEs arising form the snapshots have been broadened with a phenomenological Gaussian curve with HWHM=0.05 eV. For emission, the spectra arising from the *trans* and *cis* trajectories have been weighted with their relative weights (see text). Notice that the second band observed in the experiment is not reproduced by our calculations since we only considered transitions to the lowest excited state.

101, where however absorption was only reported in dioxane. In order to perform a more direct comparison, the absorption spectrum in ethanol has been recorded again at University of Málaga. For emission the *trans* and *cis* contributions have been weighted with the S0 populations (4:1), assuming that the radiative process is faster than photoisomerization. The agreement with experiment is perfect for absorption and still excellent for emission although some fine details of the experimental shape are not fully captured. In particular we nicely reproduce (with a slight overestimation) the larger width of the absorption with respect to emission. The full width at half maximum for absorption and emission is 0.61 and 0.52 eV, respectively, to be compared with the experimental data 0.59 and 0.54 eV. Com-

parison with the predictions of the standard CEA-VE procedure shows that the latter strongly underestimates the spectral widths and is remarkably outperformed by the new $Ad-MD|gVH$ method.

4.4 Cyanidin

Cyan molecule in water is the most challenging test for the applicability of our $Ad-MD|gVH$ protocol, because it is a charged species characterized by several flexible torsions, including the one around the C–C bond that connects the two rings and the five hydroxyl groups, H-bonded to solvent molecules. The numerous hydroxyl groups can be also easily deprotonated, creating a mixture of different species that clearly has an effect on the spectrum. For this reason we decided to focus on the comparison with the experimental spectrum in water at pH 1, where the **Cyan** dye is expected to be fully protonated. Different studies point out that in very acidic solutions the flavylium cation of **Cyan** is the only chemical species present,[102] whereas at larger pH some new structures appears by deprotonation or hydrolysis.[103] All the intra-molecular QMD-FF parameters for **Cyan** were taken from ref. 52, where a detailed comment of the quality of the results can be found. As already mentioned and discussed in Section S3.5 of the SI, **Cyan** is not a neutral species, hence RESP charges were used instead of the original CM5 ones. Moreover, since the simulations in Ref. [52] were carried out in ethanol, MD runs in water were purposely performed in this work. In order to better describe the dynamics of the several expected solute-solvent H-bonds, we run a full unconstrained MD trajectory, adopting for the water solvent the flexible SPC-Fw model.[104] Finally, it should be mentioned that, to reach electro-neutrality of the whole solvated systems, a Cl^- counterion was included in the simulations: in all selected snapshots, such counterion was always found in the large sphere treated with EE scheme but never

in the first-neighbor shell, therefore the Cl contribution to the different spectra was always treated within the EE scheme.

Table 1 shows that for more than 20% of the snapshots, a harmonic expansion of the PES is characterized by at least an imaginary frequency if the vibrational analysis is performed in Full space. Due to the flexibility of the molecule this result was expected. As a first step to apply our $Ad-MD|gVH$ method, we moved the soft torsions δ_1 to δ_6 (see expressions (28)-(33) in the SI for definition) in the classical set. In the rmTors space the number of imaginary frequencies is strongly reduced, but still for 6% of the snapshots the local PES expansions on S0 features an imaginary frequency. As it was already shown for **T2**, also for **Cyan** the flexibility associated to the inter-ring torsion is actually more complex than the simple rotation described by the flexible dihedral δ_6. In fact, further vibrational analysis on the off-equilibrium structures along MD sampling shows modes with imaginary frequencies with strong contributions from the pyramidalization of the Carbon atoms defining the rotatable bond. The ζ_1 and ζ_2 DoFs have been removed adopting the definitions given in equation (34) if the SI. Within this reduced space (rm[Tors+pyr]), the number of problematic snapshots is very limited (1 for S0 and 2 for S1) and can be safely discarded in the calculation. This example shows that the $Ad-MD|gVH$ approach can be successfully applied even in these challenging cases.

The spectra computed for all snapshots are plotted in Figure 10, showing that as for **MQ** and **T2**, they all exhibit pronounced vibronic progressions and both their shape and position depend on the specific snapshots. The smearing out of the vibronic peaks (which are not observed in the experiment), naturally arises considering their average, without the need for any phenomenological broadening. Figure 11 compares the $Ad-MD|gVH$ spectrum with the experimental one mea-

sured in water at pH 1.[105] In line with the results achieved for **MQ** and **T2**, a good agreement with experiment appears also for **Cyan**, with a slight underestimation of the tail at higher energies. Yet, the improvement of the $Ad-MD|gVH$ approach with respect to the standard CEA-VE procedure is still evident and both the width and the asymmetry of the experimental band are better reproduced.

A second band is visible in the blue wing of the experimental spectrum. Therefore we applied our $Ad-MD|gVH$ approach also to the S0→S2 transition. A larger percentage of snapshots ($\sim$ 40 %) exhibited imaginary frequencies and were discarded, signaling that the more the states are excited the more they can suffer from anhmaronic effects, or inter-state couplings that challenge the straightforward

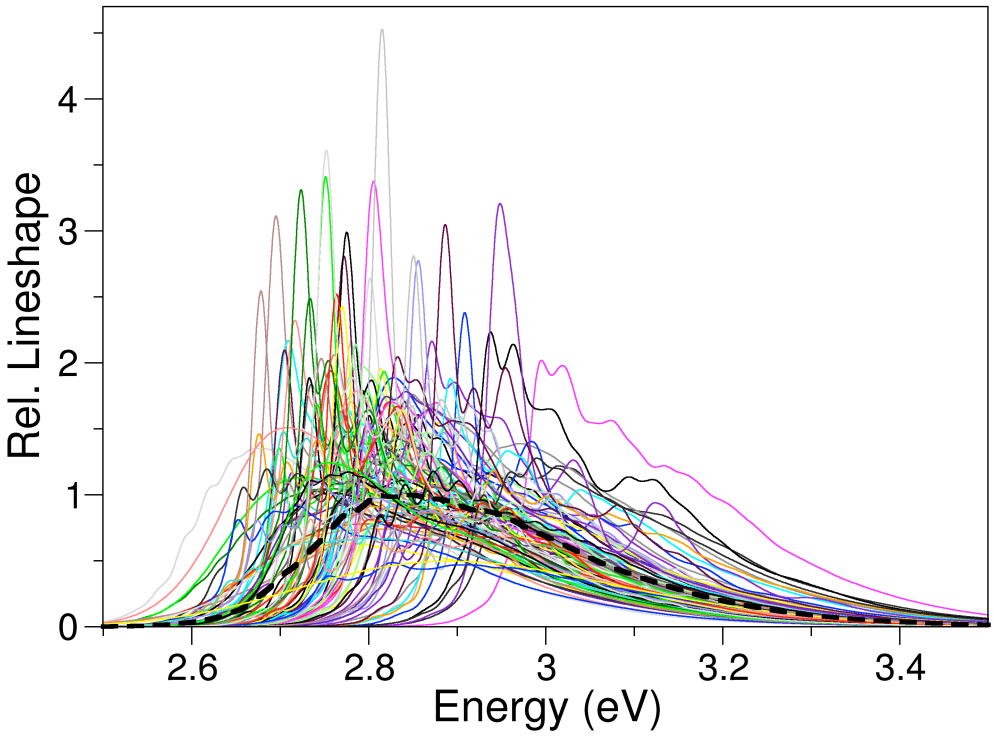

Figure 10: Vibronic spectra for the S0→S1 transition, computed for each individual snapshot along **Cyan** MD trajectory. The average spectrum is also plotted (black dashed line). Similar results were obtained for the S0→S2 transition (data not shown).

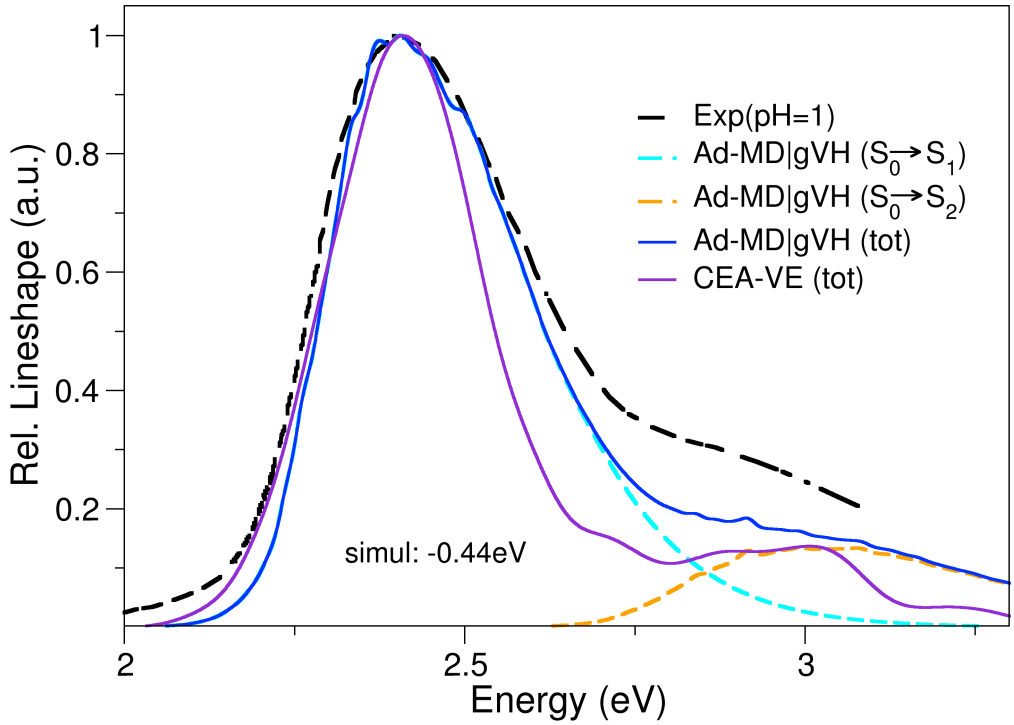

Figure 11: The absorption spectrum simulated for **Cyan** with the $Ad-MD|gVH$ approach presented in this work is compared to the experimental spectrum measured in water at pH 1.[105] A simpler simulation of the spectrum obtained with the standard CEA-VE approach, broadened with a phenomenological Gaussian curve with HWHM=0.05 eV, in analogy with what done by some of us in Ref[52] is also shown.

application of our method. This notwithstanding, Figure 11 shows that inclusion of S0→S2 contribution significantly improves the agreement with experiment. Yet, minor differences remain and they mainly concern the underestimation of: (i) the relative intensity of the blue-side shoulder, and (ii) the intensity between the two bands. The statistical analysis of the different snapshots reported in section S6 of the SI shows that when the oscillator strength of S1 decreases, the one of S2 increases, this occurring more frequently when the two states are closer in energy. This finding clearly suggests that the two states are coupled. The distance between the maximum and the blue-side shoulder is also slightly overestimated in

our computations. It is therefore plausible that an electronic method able to better reproduce this gap would also predict a stronger coupling between the two states and, therefore, a larger relative intensity of the blue-side shoulder, which would improve both points (*i*) and (*ii*). Moreover, a significant coupling between the two states should be accounted explicitly with a nonadiabatic Hamiltonian, like a LVC or a QVC model.[25] We have recently shown that one of the main effects of inter-state couplings is to increase the relative intensity between the two coupled bands.[27]

5 Discussion and Conclusions

In this contribution we presented a general *mqc* method, that we named $Ad-MD|gVH$, to compute the shape of electronic spectra of a flexible molecule in condensed phase. $Ad-MD|gVH$ is the result of a long-lasting project and builds up on previous steps we reported in recent papers, like the demonstration of the necessity of QMD-FF for spectroscopic accuracy,[7] and the description of the VH model in curvilinear internal coordinates.[70] It shares the basic idea of the classical/quantum partition within an adiabatic approximation with the few-classical-coordinates models we presented in refs.[62,106] Its main innovation is the introduction of a coherent scheme to combine MD sampling and vibronic calculations which allows to treat all the flexible coordinates of the solute and all the environment explicitly, and a generalization of the projectors to separate soft and fast coordinates. In this way, while in its current applications we considered dyes solvated in simple solvents, the method is ready to be extended to deal also with heterogeneous media, like proteins and surfaces.

The soft/stiff classical/quantum partition is a key of the $Ad-MD|gVH$

method. It is made on the grounds of chemical knowledge to predict flexible coordinates and is supported by the computational analysis to parameterize the QMD-FF and by the analysis of the MD. Moreover, it is finally revised with the goal to not include modes with imaginary frequencies in the quantum set. On this respect, it is noteworthy that the model computations in the SI on a reference harmonic models suggest that the shift of few coordinates with sufficiently low frequency between the two sets do not alter the quality of the results since, actually, both quantum and classical modes contribute to the shape and width of the computed spectra. Clearly, the $Ad-MD|gVH$ method cannot reproduce individual vibronic peaks of the soft modes, therefore it is tailored for spectra whose frequency resolution is less that the typical vibrational spacing of these modes. For these spectra however, it allows to approximately account for the effects of the coupling between the classical and quantum modes introducing, in a non-phenomenological way, both the broadening and the modulation of the quantum spectral shapes due to the soft modes.

Considering the computational cost of the whole $Ad-MD|gVH$ protocol, some steps are in common with a standard CEA-VE calculation, namely the parameterization of the QMD-FFs with Joyce program, which is rather automatized and for non-difficult cases can be planned and concluded in 1-2 days and the typical times to run a few nanoseconds MD. The additional cost of $Ad-MD|gVH$ method comes from the QM:MM computations of the ground and excited states gradients and Hessians, mostly the latter, which depending on the system and the level of theory selected has ranged from some minutes (**MQ**) to few hours (**Cyan**) on 16-cores Xeon CPUs. This operation must be repeated for the number of snapshots necessary to obtain a converged average. On this respect, in Section S7 of the SI we show that for **MQ** and **T2** the spectra are fully converged even considering half

of the 200 initial snapshots, and that for **Cyan** adopting only 50 of the computed 100 snapshots leads to only small discrepancies. It is noteworthy that alternative protocols to drastically reduce the computational cost are conceivable and their performance will be investigated in future work.

In these first applications of $Ad-MD|gVH$, we computed absorption and emission spectra, but in principle the method is suited for any other electronic spectroscopy like electronic circular dichroism, magnetic circular dichroism, circularly polarized luminescence, Resonance Raman, non-resonant two-photon absorption and others, for those systems for which couplings among the electronic states are negligible or can be accounted for perturbatively, within HT theory. When electronic couplings are strong it is conceivable to extend the $Ad-MD|gVH$ method substituting the gVH engine with LVC or QVC models in reduced dimensionality.

In the implementation adopted here, we made a number of computational choices regarding the MD, the adopted FFs, the electronic method and the embedding scheme in QM/MM calculations that are not fundamental for the $Ad-MD|gVH$ method. The latter in fact is in principle versatile enough and ready to be combined with alternative settings. In the MD, for the solute we used a QMD-FF, fitted against data obtained at the same level of theory adopted to generate harmonic PESs for vibronic calculations. This ensures that the procedure is consistent and that, along the MD, the system does not visit unrealistic configurations where also the data needed for vibronic models might be biased and unreliable. Similar problems have been encountered several times with standard empirical FFs, which do not guarantee spectroscopic precision. They have been cured with different strategies, like a re-optimization of the solute at each snapshot,[107] which however reduces the conformational sampling and might introduce unreliable solute-solvent configurations. The problems arising from structures ex-

tracted with inaccurate FFs, already seen on vertical transitions,[7] would be even more important in $Ad-MD|gVH$, where higher-order properties of the PESs, like energy gradients and Hessians, are needed.

Alternative strategies might be implemented in the same $Ad-MD|gVH$ scheme, like QM/MM trajectories, taking care that the propagation time is long enough for an accurate spanning of the configurational space, or refinements of the samplings with short QM/MM trajectories, run at selected configurations obtained with a classical FF, to ensure that faster modes do oscillate around reasonable geometries.[108] A further possible development in the classical MD is to use QMD-FFs also for the solute-environment parameters, along the lines recently proposed by some of us.[109]

It is noteworthy that some steps of $Ad-MD|gVH$ method, namely the MD simulation followed by the computation of harmonic PES of the stiff coordinates, specific for each configuration, shares analogies with what proposed by Lee et al.[63] for computing spectral densities of chromophores in complex environments. In fact they obtain such density by the excited state gradient at the optimized geometries of the chromophore in a number of environmental configurations (our soft modes). Advantages of our method are the explicit inclusion of quadratic differences of initial and final state PESs, and the larger flexibility in defining soft and stiff modes. Always concerning the sampling, in the future it will be interesting to try to combine our approach to more elaborated samplings, like those adopted by Rosa et al.[110]

As far as the embedding scheme is considered, we adopted an ONIOM QM:MM model. It is possible in principle to couple our method with more sophisticated polarizable embedding schemes.[107,111–113] or with the cost-effective Perturbation Matrix Method (PMM).[114] On this respect, we mention that a very recent contri-

bution introduced an hybrid approach based on a clustering technique that adopts ONIOM/EE for a representative structure of each cluster and the faster PMM approach for local fluctuations in each cluster.[115] It will be interesting to investigate in future works effective ways to combine this approach with vibronic calculations and the effect of clustering techniques on the reproduction of the solute-solvent broadening effects of the electronic spectra. Finally, while we adopted a classical MD, the combination of $Ad-MD|gVH$ with a path-integral MD, able to account for NQEs along the lines proposed refs. 55 and 66, is doable and would be surely of large interest.

Acknowledgements

This work has received funding from the European Union's Horizon 2020 research and innovation programme MSCA-ITN under grant agreement No. 765266 (LightDyNAmics).. Computational resources provided by the Centro de Cálculo Científico at Universidad Autónoma de Madrid (CCC-UAM) and by SCBI (Supercomputing and Bioinformatics) center of Universidad de Málaga are also acknowledged. DA and FA thank financial support from Spanish "Ministerio de Economía y Competitividad" (Project CTQ2015-65816-R). DA acknowledges Fundación Ramón Areces (Spain) for funding his postdoctoral stay at ICCOM-CNR Pisa. JC and DA acknowledge the Pisa Unit of ICCOM-CNR Pisa for hospitality.

Supporting Information

Comparison of $Ad-MD|gVH$ and fully quantum spectra for harmonic models. Details on the parametrization and the snapshot sampling. Definition of curvilinear coordinates removed for the different molecules and further analysis on the

occurrence of imaginary frequencies. Check of the effect of the broadening over individual spectra. Analysis of the effects of the point charges and S1/S2 coupling in **Cyan**. This information is available free of charge via the Internet at http://pubs.acs.org

References

(1) Jensen, P.; Bunker, P. R. *Computational Molecular Spectroscopy*; Wiley, Chichester, England, 2000.

(2) Barone, V. *Computational Strategies for Spectroscopy: From Small Molecules to Nano Systems*; Wiley, Hoboken, NJ, 2011.

(3) Barone, V. The virtual multifrequency spectrometer: a new paradigm for spectroscopy. *WIREs Comput. Mol. Sci.* **2016**, *6*, 86–110.

(4) Lax, M. The Franck-Condon Principle and Its Application to Crystals. *J. Chem. Phys.* **1952**, *20*, 1752–1760.

(5) Avila Ferrer, F. J.; Cerezo, J.; Stendardo, E.; Improta, R.; Santoro, F. Insights for an Accurate Comparison of Computational Data to Experimental Absorption and Emission Spectra: Beyond the Vertical Transition Approximation. *J. Chem. Theory Comput.* **2013**, *9*, 2072–2082.

(6) Petrone, A.; Cerezo, J.; Ferrer, F. J. A.; Donati, G.; Improta, R.; Rega, N.; Santoro, F. Absorption and Emission Spectral Shapes of a Prototype Dye in Water by Combining Classical/Dynamical and Quantum/Static Approaches. *J. Phys. Chem. A* **2015**, *119*, 5426–5438, PMID: 25699575.

(7) Cerezo, J.; Santoro, F.; Prampolini, G. Comparing classical approaches with empirical or quantum-mechanically derived force fields for the simulation electronic lineshapes: application to coumarin dyes. *Theor. Chem. Acc.* **2016**, *135*, 135–143.

(8) Eroms, M.; Jungen, M.; Meyer, H.-D. Vibronic Coupling Effects in Resonant Auger Spectra of H2O. *J. Phys. Chem. A* **2012**, *116*, 11140–11150.

(9) Dierksen, M.; Grimme, S. An efficient approach for the calculation of Franck–Condon integrals of large molecules. *J. Chem. Phys.* **2005**, *122*, 244101.

(10) Hazra, A.; Nooijen, M. Derivation and Efficient Implementation of a Recursion Formula to Calculate Harmonic Franck-Condon Factors for Polyatomic Molecules. *Int. J. Quantum Chem.* **2003**, *95*, 643–657.

(11) Santoro, F.; Improta, R.; Lami, A.; Bloino, J.; Barone, V. Effective method to compute Franck-Condon integrals for optical spectra of large molecules in solution. *J. Chem. Phys.* **2007**, *126*, 084509.

(12) Santoro, F.; Lami, A.; Improta, R.; Bloino, J.; Barone, V. Effective method for the computation of optical spectra of large molecules at finite temperature including the Duschinsky and Herzberg–Teller effect: The Qx band of porphyrin as a case study. *J. Chem. Phys.* **2008**, *128*, 224311.

(13) Jankowiak, H.-C.; Stuber, J. L.; Berger, R. Vibronic transitions in large molecular systems: Rigorous prescreening conditions for Franck-Condon factors. *J. Chem. Phys.* **2007**, *127*, 234101.

(14) Tang, J.; Lee, M. T.; Lin, S. H. Effects of the Duschinsky mode-mixing mechanism on temperature dependence of electron transfer processes. *J. Chem. Phys.* **2003**, *119*, 7188–7196.

(15) Ianconescu, R.; Pollak, E. Photoinduced Cooling of Polyatomic Molecules in an Electronically Excited State in the Presence of Dushinskii Rotations. *J. Phys. Chem. A* **2004**, *108*, 7778–7784.

(16) Tatchen, J.; Pollak, E. Ab initio spectroscopy and photoinduced cooling of the trans-stilbene molecule. *J. Chem. Phys.* **2008**, *128*, 164303.

(17) Lami, A.; Santoro, F. In *Computational Strategies for Spectroscopy*; Barone, V., Ed.; John Wiley & Sons, Inc., 2011; Chapter 10, pp 475–516.

(18) Peng, Q.; Niu, Y.; Deng, C.; Shuai, Z. Vibration correlation function formalism of radiative and non-radiative rates for complex molecules. *Chem. Phys.* **2010**, *370*, 215–222.

(19) Borrelli, R.; Capobianco, A.; Peluso, A. Generating Function Approach to the Calculation of Spectral Band Shapes of Free-Base Chlorin Including Duschinsky and Herzberg-Teller Effects. *J. Phys. Chem. A* **2012**, *116*, 9934–9940.

(20) Huh, J.; Berger, R. Coherent state-based generating function approach for Franck-Condon transitions and beyond. *J. Phys.: Conf. Ser.* **2012**, *380*, 012019.

(21) Baiardi, A.; Bloino, J.; Barone, V. General Time Dependent Approach to Vibronic Spectroscopy Including Franck-Condon, Herzberg-Teller, and Duschinsky Effects. *J. Chem. Theory Comput.* **2013**, *9*, 4097–4115.

(22) Avila Ferrer, F. J.; Cerezo, J.; Soto, J.; Improta, R.; Santoro, F. First-principle computation of absorption and fluorescence spectra in solution accounting for vibronic structure, temperature effects and solvent inhomogenous broadening. *Comput. Theoret. Chem.* **2014**, *1040–1041*, 328–337.

(23) Etinski, M.; Rai-Constapel, V.; Marian, C. M. Time-dependent approach to spin-vibronic coupling: Implementation and assessment. *J. Chem. Phys.* **2014**, *140*.

(24) Jacquemin, D.; Adamo, C. In *Density-Functional Methods for Excited*

States; Ferré, N., Filatov, M., Huix-Rotllant, M., Eds.; Springer International Publishing: Cham, 2016; pp 347–375.

(25) Köppel, H.; Domcke, W.; Cederbaum, L. The Multi-mode vibronic-coupling approach . Conical Intersections, Electronic Structure, Dynamics and Spectroscopy. 2004; pp 323–368.

(26) Meng, Q.; Meyer, H.-D. A multilayer MCTDH study on the full dimensional vibronic dynamics of naphthalene and anthracene cations. *J. Chem. Phys.* **2013**, *138*, 014313.

(27) Liu, Y.; Martínez-Fernández, L.; Cerezo, J.; Prampolini, G.; Improta, R.; Santoro, F. Multistate coupled quantum dynamics of photoexcited cytosine in gas-phase: Nonadiabatic absorption spectrum and ultrafast internal conversions. *Chem. Phys.* **2018**, *515*, 452–463.

(28) Beck, M. H.; Jäckle, A.; Worth, G. A.; Meyer, H.-D. The multiconfiguration time-dependent Hartree method: A highly efficient algorithm for propagating wavepackets. *Phys. Rep.* **2000**, *324*, 1–105.

(29) Wang, H.; Thoss, M. Multilayer formulation of the multiconfiguration time-dependent Hartree theory. *J. Chem. Phys.* **2003**, *119*, 1289–1299.

(30) Vendrell, O.; Meyer, H.-D. Multilayer multiconfiguration time-dependent Hartree method: Implementation and applications to a Henon-Heiles Hamiltonian and to pyrazine. *J. Chem. Phys.* **2011**, *134*, 044135.

(31) Christiansen, O. Vibrational structure theory: new vibrational wave function methods for calculation of anharmonic vibrational energies and vibrational contributions to molecular properties. *Phys. Chem. Chem. Phys.* **2007**, *9*, 2942–2953.

(32) Császá, A. G. Anharmonic molecular force fields. *WIREs Comput. Mol. Sci.* *2*, 273–289.

(33) Barone, V. Anharmonic vibrational properties by a fully automated second-order perturbative approach. *J. Chem. Phys.* **2005**, *122*, 014108.

(34) Bloino, J.; Biczysko, M.; Barone, V. General Perturbative Approach for Spectroscopy, Thermodynamics, and Kinetics: Methodological Background and Benchmark Studies. *J. Chem. Theory Comput.* **2012**, *8*, 1015–1036.

(35) Egidi, F.; Williams-Young, D. B.; Baiardi, A.; Bloino, J.; Scalmani, G.; Frisch, M. J.; Li, X.; Barone, V. Effective Inclusion of Mechanical and Electrical Anharmonicity in Excited Electronic States: VPT2-TDDFT Route. *J. Chem. Theory Comput.* **2017**, *13*, 2789–2803, PMID: 28453287.

(36) Madsen, D.; Christiansen, O.; Norman, P.; König, C. Vibrationally resolved emission spectra of luminescent conjugated oligothiophenes from anharmonic calculations. *Phys. Chem. Chem. Phys.* **2019**, *21*, 17410–17422.

(37) Zuehlsdorff, T. J.; Montoya-Castillo, A.; Napoli, J. A.; Markland, T. E.; Isborn, C. M. Optical spectra in the condensed phase: Capturing anharmonic and vibronic features using dynamic and static approaches. *J. Chem. Phys.* **2019**, *151*, 074111.

(38) Mennucci, B.; Cappelli, C.; Guido, C. A.; Cammi, R.; Tomasi, J. Structures and Properties of Electronically Excited Chromophores in Solution from the Polarizable Continuum Model Coupled to the Time-Dependent Density Functional Theory. *J. Phys. Chem. A* **2009**, *113*, 3009–3020, PMID: 19226132.

(39) Charaf-Eddin, A.; Planchat, A.; Mennucci, B.; Adamo, C.; Jacquemin, D. Choosing a Functional for Computing Absorption and Fluorescence Band Shapes with TD-DFT. *J. Chem. Theory Comput.* **2013**, *9*, 2749–2760.

(40) Tomasi, J.; Mennucci, B.; Cammi, R. Quantum Mechanical Continuum Solvation Models. *Chem. Rev.* **2005**, *105*, 2999–3094.

(41) Bergsma, J. P.; Berens, P. H.; Wilson, K. R.; Fredkin, D. R.; Heller, E. J. Electronic spectra from molecular dynamics: a simple approach. *J. Phys. Chem.* **1984**, *88*, 612–619.

(42) Canuto, E., S. *Solvation Effects on Molecules and Biomolecules. Computational Methods and Applications*; Springer, 2008.

(43) Marini, A.; Muñoz-Losa, A.; Biancardi, A.; Mennucci, B. What is solvatochromism? *J. Phys. Chem. B* **2010**, *114*, 17128–35.

(44) Sabin, J. R.; Brändas, E. E. *Combining Quantum Mechanics and Molecular Mechanics. Some Recent Progresses in QM/MM Methods, Advances in Quantum Chemistry*; Elsevier, 2010.

(45) Murugan, N. A.; Rinkevicius, Z.; Ågren, H. Modeling solvatochromism of Nile red in water. *Int. J. Quantum Chem.* **2011**, *111*, 1521–1530.

(46) Marenich, A. V.; Cramer, C. J.; Truhlar, D. G. Electronic Absorption Spectra and Solvatochromic Shifts by the Vertical Excitation Model: Solvated Clusters and Molecular Dynamics Sampling. *J. Phys. Chem. B* **2015**, *119*, 958–967.

(47) Brunk, U., E.and Rothlisberger Mixed Quantum Mechanical/Molecular Me-

chanical Molecular Dynamics Simulations of Biological Systems in Ground and Electronically Excited States. *Chem. Rev.* **2015**, *115*, 6217–6263.

(48) Zuehlsdorff, T. J.; Isborn, C. M. Modeling absorption spectra of molecules in solution. *Int. J. Quantum Chem.* **2019**, *119*, e25719.

(49) Caputo, M. C.; Provasi, P. F.; Benitez, L.; Georg, H. C.; Canuto, S.; Coutinho, K. Monte Carlo–Quantum Mechanics Study of Magnetic Properties of Hydrogen Peroxide in Liquid Water. *J. Phys. Chem. A* **2014**, *118*, 6239–6247.

(50) De Mitri, N.; Monti, S.; Prampolini, G.; Barone, V. Absorption and Emission Spectra of a Flexible Dye in Solution: A Computational Time-Dependent Approach. *J. Chem. Theory Comput.* **2013**, *9*, 4507–4516.

(51) Chandrasekaran, S.; Aghtar, M.; Valleau, S.; Aspuru-Guzik, A.; Kleinekathöfer, U. Influence of Force Fields and Quantum Chemistry Approach on Spectral Densities of BChl a in Solution and in FMO Proteins. *J. Phys. Chem. B* **2015**, *119*, 9995–10004.

(52) Cacelli, I.; Ferretti, A.; Prampolini, G. Predicting light absorption properties of anthocyanidins in solution: a multi-level computational approach. *Theor. Chem. Acc.* **2016**, *135*, 156.

(53) Andreussi, O.; Prandi, I. G.; Campetella, M.; Prampolini, G.; Mennucci, B. Classical Force Fields Tailored for QM Applications: Is It Really a Feasible Strategy? *J. Chem. Theor. and Comput.* **2017**, *13*, 4636–4648.

(54) Eilmes, A. Effect of Molecular Vibrations on the MD/QC-Simulated Absorption Spectra. *Int. J. Quantum Chem.* **2014**, *114*, 261–270.

(55) Law, Y. K.; Hassanali, A. A. The importance of nuclear quantum effects in spectral line broadening of optical spectra and electrostatic properties in aromatic chromophores. *J. Chem. Phys.* **2018**, *148*, 102331.

(56) Craig, I. R.; Manolopoulos, D. E. Quantum statistics and classical mechanics: Real time correlation functions from ring polymer molecular dynamics. *J. Chem. Phys.* **2004**, *121*, 3368–3373.

(57) Tatchen, J.; Pollak, E. Semiclassical on-the-fly computation of the S0â†'S1 absorption spectrum of formaldehyde. *J. Chem. Phys.* **2009**, *130*, 041103.

(58) D'Alessandro, M.; Aschi, M.; Mazzuca, C.; Palleschi, A.; Amadei, A. Theoretical modeling of UV-Vis absorption and emission spectra in liquid state systems including vibrational and conformational effects: The vertical transition approximation. *J. Chem. Phys.* **2013**, *139*, 114102.

(59) D'Abramo, M.; Aschi, M.; Amadei, A. Theoretical modeling of UV-Vis absorption and emission spectra in liquid state systems including vibrational and conformational effects: Explicit treatment of the vibronic transitions. *J. Chem. Phys.* **2014**, *140*, 164104.

(60) Zalenśy, R.; Murugan, N. A.; Gelmukhanov, F.; Rinkevicius, Z.; Ośmialowski, B.; Bartkowiak, W.; Ågren, H. Toward Fully Nonempirical Simulations of Optical Band Shapes of Molecules in Solution: a Case Study of Heterocyclic Ketoimine Difluoroborates. *J. Phys. Chem. A* **2015**, *119*, 5145–5152.

(61) Cerezo, J.; Ferrer, F. J. A.; Prampolini, G.; Santoro, F. Modeling Solvent Broadening on the Vibronic Spectra of a Series of Coumarin Dyes. From

Implicit to Explicit Solvent Models. *J. Chem. Theory Comput.* **2015**, *11*, 5810–5825.

(62) Cerezo, J.; Aranda, D.; Avila Ferrer, F. J.; Prampolini, G.; Mazzeo, G.; Longhi, G.; Abbate, S.; Santoro, F. Toward a general mixed quantum/classical method for the calculation of the vibronic ECD of a flexible dye molecule with different stable conformers: Revisiting the case of 2,2,2-trifluoro-anthrylethanol. *Chirality 30*, 730–743.

(63) Lee, M. K.; Coker, D. F. Modeling Electronic-Nuclear Interactions for Excitation Energy Transfer Processes in Light-Harvesting Complexes. *J. Phys. Chem. Lett.* **2016**, *7*, 3171–3178.

(64) Loco, D.; Cupellini, L. Modeling the absorption lineshape of embedded systems from molecular dynamics: A tutorial review. *Int. J. Quantum Chem.* **2019**, *119*, e25726.

(65) Zuehlsdorff, T. J.; Isborn, C. M. Combining the ensemble and Franck-Condon approaches for calculating spectral shapes of molecules in solution. *J. Chem. Phys.* **2018**, *148*, 024110.

(66) Zuehlsdorff, T. J.; Napoli, J. A.; Milanese, J. M.; Markland, T. E.; Isborn, C. M. Unraveling electronic absorption spectra using nuclear quantum effects: Photoactive yellow protein and green fluorescent protein chromophores in water. *J. Chem. Phys.* **2018**, *149*, 024107.

(67) Cacelli, I.; Prampolini, G. Parametrization and Validation of Intramolecular Force Fields Derived from DFT Calculations. *J. Chem. Theor. Comput.* **2007**, *3*, 1803–1817.

(68) Barone, V.; Cacelli, I.; De Mitri, N.; Licari, D.; Monti, S.; Prampolini, G. Joyce and Ulysses: integrated and user-friendly tools for the parameterization of intramolecular force fields from quantum mechanical data. *Phys. Chem. Chem. Phys.* **2013**, *15*, 3736–3751.

(69) Cerezo, J.; Prampolini, G.; Cacelli, I. Developing accurate intramolecular force fields for conjugated systems through explicit coupling terms. *Theor. Chem. Acc.* **2018**, *137*, 80.

(70) Cerezo, J.; Santoro, F. Revisiting Vertical Models To Simulate the Line Shape of Electronic Spectra Adopting Cartesian and Internal Coordinates. *J. Chem. Theory Comput.* **2016**, *12*, 4970–4985.

(71) Duschinsky, F. On the Interpretation of Electronic Spectra of Polyatomic Molecules. I. The Franck-Condon Principle. *Acta Physicochim.: URSS* **1937**, *7*, 551–566.

(72) Santoro, F.; Cerezo, J. $\mathcal{FC}classes3$, a code for vibronic calculations. Available upon request. 2019.

(73) Avila Ferrer, F. J.; Santoro, F. Comparison of vertical and adiabatic harmonic approaches for the calculation of the vibrational structure of electronic spectra. *Phys. Chem. Chem. Phys.* **2012**, *14*, 13549–13563.

(74) Brandhorst, K.; Grunenberg, J. Efficient computation of compliance matrices in redundant internal coordinates from Cartesian Hessians for nonstationary points. *J. Chem. Phys.* **2010**, *132*, 184101.

(75) Reimers, J. R. A practical method for the use of curvilinear coordinates in calculations of normal-mode-projected displacements and Duschinsky rotation matrices for large molecules. *J. Chem. Phys.* **2001**, *115*, 9103–9109.

(76) Baiardi, A.; Bloino, J.; Barone, V. Accurate Simulation of Resonance-Raman Spectra of Flexible Molecules: An Internal Coordinates Approach. *J. Chem. Theory Comput.* **2015**, *11*, 3267–3280, PMID: 26575763.

(77) Baiardi, A.; Bloino, J.; Barone, V. General formulation of vibronic spectroscopy in internal coordinates. *J. Chem. Phys.* **2016**, *144*, 084114.

(78) Jackels, C. F.; Gu, Z.; Truhlar, D. G. Reaction-path potential and vibrational frequencies in terms of curvilinear internal coordinates. *J. Chem. Phys.* **1995**, *102*, 3188–3201.

(79) Sands, D. *Vectors and Tensors in Crystallography*; Addison-Weley: Reading, MA, 1982.

(80) Aranda, D.; Cerezo, J.; Pescitelli, G.; Avila Ferrer, F. J.; Soto, J.; Santoro, F. A computational study of the vibrationally-resolved electronic circular dichroism spectra of single-chain transoid and cisoid oligothiophenes in chiral conformations. *Phys. Chem. Chem. Phys.* **2018**, *20*, 21864–21880.

(81) Wilson, Jr., E. B. Some Mathematical Methods for the Study of Molecular Vibrations. *J. Chem. Phys.* **1941**, *9*, 76–84.

(82) Wilson, E. B.; Decius, J. C.; Cross, P. C. *Molecular Vibrations. The Theory of Infrared and Raman Vibrational Spectra*; Dover, 1955.

(83) Frisch, M. J. et al. Gaussian˜16 Revision B.01. 2016; Gaussian Inc. Wallingford CT.

(84) Pronk, S. et al. GROMACS 4.5: a High-Throughput and Highly Parallel Open Source Molecular Simulation Toolkit. *Bioinformatics* **2013**, *29*, 845–854.

(85) Abraham, M. J.; Murtola, T.; Schulz, R.; Páll, S.; Smith, J. C.; Hess, B.; Lindahl, E. GROMACS: High performance molecular simulations through multi-level parallelism from laptops to supercomputers. *SoftwareX* **2015**, *1-2*, 19 – 25.

(86) Cacelli, I.; Cerezo, J.; ; De Mitri, N.; Prampolini, G. JOYCE2.10, a Fortran 77 code for intra-molecular force field parameterization. , available free of charge at http://www.pi.iccom.cnr.it/joyce, last consulted November. 2019.

(87) Santoro, F. $\mathcal{FC}classes$, a Fortran 77 code for vibronic calculations, visit: http://www.pi.iccom.cnr.it/fcclasses, last consulted November. 2019.

(88) Stendardo, E.; Avila Ferrer, F.; Santoro, F.; Improta, R. Vibrationally Resolved Absorption and Emission Spectra of Dithiophene in the Gas Phase and in Solution by First-Principle Quantum Mechanical Calculations. *J. Chem. Theory Comput.* **2012**, *8*, 4483–4493.

(89) Marenich, A. V.; Jerome, S. V.; Cramer, C. J.; Truhlar, D. G. Charge Model 5: An Extension of Hirshfeld Population Analysis for the Accurate Description of Molecular Interactions in Gaseous and Condensed Phases. *J. Chem. Theor. Comput.* **2012**, *8*, 527–541.

(90) Bayly, C. I.; Cieplak, P.; Cornell, W.; Kollman, P. A. A well-behaved electrostatic potential based method using charge restraints for deriving atomic charges: the RESP model. *J. Phys. Chem.* **1993**, *97*, 10269–10280.

(91) Bultinck, P.; Van Alsenoy, C.; Ayers, P. W.; Carbó-Dorca, R. Critical analysis and extension of the Hirshfeld atoms in molecules. *J. Chem. Phys.* **2007**, *126*, 144111.

(92) Jorgensen, W. L.; Maxwell, D. S.; Tirado-rives, J. Development and Testing of the OPLS All-Atom Force Field on Conformational Energetics and Properties of Organic Liquids. *J. Am. Chem. Soc.* **1996**, *7863*, 11225–11236.

(93) Damm, W.; Frontera, A.; Tirado-Rives, J.; Jorgensen, W. L. OPLS all-atom force field for carbohydrates. *J. Comp. Chem.* **1997**, *18*, 1955–1970.

(94) Jorgensen, W. L.; Tirado-Rives, J. Potential Energy Functions for Atomic-Level Simulations of Water and Organic and Biomolecular Systems. *Proc. Natl. Acad. Sci. USA* **2005**, *102*, 6665–70.

(95) Hess, B.; Bekker, B.; Berendsen, H.; J.G.E.M., F. LINCS: A linear constraint solver for molecular simulations. *J. Comp. Chem.* **1997**, *18*, 1463 – 1472.

(96) Bussi, G.; Donadio, D.; Parrinello, M. Canonical sampling through velocity rescaling. *J. Chem. Phys.* **2007**, *126*, 014101.

(97) Parrinello, M.; Rahman, A. Polymorphic transitions in single crystals: A new molecular dynamics method. *J. Appl. Phys.* **1981**, *52*, 7182–7190.

(98) Prampolini, G.; Ingrosso, F.; Cerezo, J.; Iagatti, A.; Foggi, P.; Pastore, M. Short- and Long-Range Solvation Effects on the Transient UV–Vis Absorption Spectra of a Ru(II)–Polypyridine Complex Disentangled by Nonequilibrium Molecular Dynamics. *J. Phys. Chem. Lett.* **2019**, *10*, 2885–2891.

(99) Miyamoto, S.; Kollman, P. SETTLE: An analytical version of the SHAKE and RATTLE algorithms for rigid water models. *J. Comp. Chem.* **1992**, *13*, 952 – 962.

(100) Schnappinger, T.; Marazzi, M.; Mai, S.; Monari, A.; González, L.; de Vivie-Riedle, R. Intersystem Crossing as a Key Component of the Nonadiabatic

Relaxation Dynamics of Bithiophene and Terthiophene. *J. Chem. Theory Comput.* **2018**, *14*, 4530–4540, PMID: 30091911.

(101) Becker, R. S.; Seixas de Melo, J.; Maçanita, A. L.; Elisei, F. Comprehensive Evaluation of the Absorption, Photophysical, Energy Transfer, Structural, and Theoretical Properties of α-Oligothiophenes with One to Seven Rings. *J. Phys. Chem.* **1996**, *100*, 18683–18695.

(102) Rakić, V.; Åsmund Rinnan,; Polak, T.; Skrt, M.; Miljković, M.; Ulrih, N. P. pH-induced structural forms of cyanidin and cyanidin 3-O-β-glucopyranoside. *Dyes Pigm.* **2019**, *165*, 71 – 80.

(103) Cabrita, L.; Petrov, V.; Pina, F. On the thermal degradation of anthocyanidins: cyanidin. *RSC Adv.* **2014**, *4*, 18939–18944.

(104) Wu, H., Y.and Tepper; Voth, G. Flexible Simple Point-Charge Water Model with Improved Liquid-State Properties. *J. Chem. Phys.* **2006**, *124*, 024503.

(105) Dai, Q.; Rabani, J. Photosensitization of nanocrystalline TiO2 films by anthocyanin dyes. *J. Photochem. Photobiol. A* **2002**, *148*, 17 – 24, Semiconductor Photochemistry 1 First International Conference On Semiconductor Photochemistry,University Of Strathclyde, Glasgow, July 2001.

(106) Cerezo, J.; Mazzeo, G.; Longhi, G.; Abbate, S.; Santoro, F. Quantum-Classical Calculation of Vibronic Spectra along a Reaction Path: The Case of the ECD of Easily Interconvertible Conformers with Opposite Chiral Responses. *J. Phys. Chem. Lett.* **2016**, *7*, 4891–4897.

(107) Kjellgren, E. R.; Haugaard Olsen, J. M.; Kongsted, J. Importance of Accurate Structures for Quantum Chemistry Embedding Methods: Which Strategy Is Better? *J. Chem. Theory Comput.* **2018**, *14*, 4309–4319.

(108) De Vetta, M.; Baig, O.; Steen, D.; Nogueira, J. J.; GonzÃ¡lez, L. Assessing Configurational Sampling in the Quantum Mechanics/Molecular Mechanics Calculation of Temoporfin Absorption Spectrum and Triplet Density of States. *Molecules* **2018**, *23*, 2932.

(109) Greff da Silveira, L.; Jacobs, M.; Prampolini, G.; Livotto, P. R.; Cacelli, I. Development and Validation of Quantum Mechanically Derived Force-Fields: Thermodynamic, Structural, and Vibrational Properties of Aromatic Heterocycles. *J. Chem. Theor. and Comput.* **2018**, *14*, 4884–4900.

(110) Rosa, M.; Micciarelli, M.; Laio, A.; Baroni, S. Sampling Molecular Conformers in Solution with Quantum Mechanical Accuracy at a Nearly Molecular-Mechanics Cost. *J. Chem. Theory Comput.* **2016**, *12*, 4385–4389.

(111) Giovannini, T.; Macchiagodena, M.; Ambrosetti, M.; Puglisi, A.; Lafiosca, P.; Lo Gerfo, G.; Egidi, F.; Cappelli, C. Simulating vertical excitation energies of solvated dyes: From continuum to polarizable discrete modeling. *Int. J. Quantum Chem. 119*, e25684.

(112) Steinmann, C.; Reinholdt, P.; NÃ¸rby, M. S.; Kongsted, J.; Olsen, J. M. H. Response properties of embedded molecules through the polarizable embedding model. *Int. J. Quantum Chem.* **2019**, *119*, e25717.

(113) Loco, D.; Gelfand, N.; Jurinovich, S.; Protti, S.; Mezzetti, A.; Mennucci, B. Polarizable QM/Classical Approaches for the Modeling of Solvation Effects on UV-Vis and Fluorescence Spectra: An Integrated Strategy. *J. Phys. Chem. A* **2018**, *122*, 390–397.

(114) Carrillo-Parramon, O.; Del Galdo, S.; Aschi, M.; Mancini, G.; Amadei, A.; Barone, V. Flexible and Comprehensive Implementation of MD-PMM Ap-

proach in a General and Robust Code. *J. Chem. Theory Comput.* **2017**, *13*, 5506–5514.

(115) Del Galdo, S.; Chandramouli, B.; Mancini, G.; Barone, V. Assessment of Multi-Scale Approaches for Computing UV-Vis Spectra in Condensed Phases: Toward an Effective yet Reliable Integration of Variational and Perturbative QM/MM Approaches. *Journal of Chemical Theory and Computation* **2019**, *15*, 3170–3184.

Graphical TOC Entry

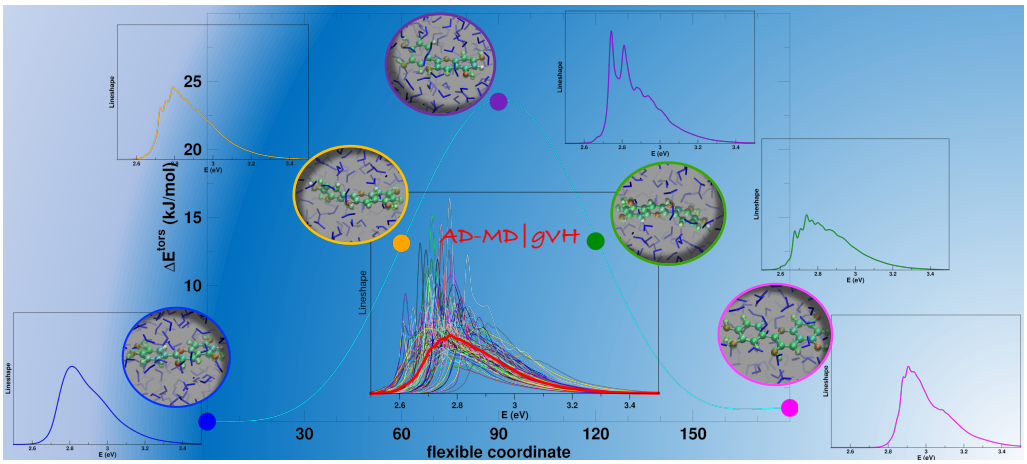

Table of Contents